Available online at www.sciencedirect.com
SCIENCE DIRECT
Physica D 219 (2006) 40–59
PHYSICA D
www.elsevier.com/locate/physd

Nature of complex singularities for the 2D Euler equation

W. Pauls[a,b], T. Matsumoto[c,a], U. Frisch[a,*], J. Bec[a]

[a] *CNRS UMR 6202, Observatoire de la Côte d'Azur, BP 4229, 06304 Nice Cedex 4, France*
[b] *Fakultät für Physik, Universität Bielefeld, Universitätsstraße 25, 33615 Bielefeld, Germany*
[c] *Department of Physics, Kyoto University, Katashirakawa Oiwakecho Sakyo-ku, Kyoto 606-8502, Japan*

Received 24 October 2005; received in revised form 6 April 2006; accepted 12 May 2006

Communicated by E. Vanden-Eijnden

Abstract

A detailed study of complex-space singularities of the two-dimensional incompressible Euler equation is performed in the short-time asymptotic régime when such singularities are very far from the real domain; this allows an exact recursive determination of arbitrarily many spatial Fourier coefficients. Using high-precision arithmetic we find that the Fourier coefficients of the stream function are given over more than two decades of wavenumbers by $\hat{F}(\boldsymbol{k}) = C(\theta)k^{-\alpha}\mathrm{e}^{-k\delta(\theta)}$, where $\boldsymbol{k} = k(\cos\theta,\ \sin\theta)$. The prefactor exponent α, typically between 5/2 and 8/3, is determined with an accuracy better than 0.01. It depends on the initial condition but not on θ. The vorticity diverges as $s^{-\beta}$, where $\alpha+\beta = 7/2$ and s is the distance to the (complex) singular manifold. This new type of non-universal singularity is permitted by the strong reduction of nonlinearity (depletion) which is associated to incompressibility. Spectral calculations show that the scaling reported above persists well beyond the time of validity of the short-time asymptotics. A simple model in which the vorticity is treated as a passive scalar is shown analytically to have universal singularities with exponent $\alpha = 5/2$.

Keywords: Euler equation; Singularities

Und es wallet und siedet und brauset und zischt,
Wie wenn Wasser mit Feuer sich mengt,
Bis zum Himmel spritzet der dampfende Gischt,
Und Flut auf Flut sich ohn' Ende drängt...
Friedrich von Schiller, from *Der Taucher* [1]

1. Introduction

A quarter of a millennium has elapsed since Euler published for the first time what is now known as the Euler equations of hydrodynamics [2]. There has not been much celebration but this may just reflect our embarrassment at not having made enough progress. Actually, Leonhard Euler warned us. At the end of his 1755 paper he wrote: "However all that the Theory of fluids holds, is contained in the two equations above, so that in the pursuit of the research we are not lacking the principles of Mechanics, but solely the Analysis, which is not yet cultivated enough for this design: hence we see clearly, which discoveries are left for us to make in this Science, before we can attain a more perfect Theory of the motion of fluids".[1] (A paper in Latin *Principia motus fluidorum*, published a few years after the paper in French, contains the basic equations and was already presented under a different title to the Berlin Academy in 1752.)

Euler considered both the compressible and incompressible cases. Here we are concerned only with the latter which is particularly difficult in view of the global nature of the incompressibility constraint. One of the most important open questions concerning the "analysis" of the Euler equations is the well-posedness: does initially smooth 3D flow, which is known to remain smooth for short times, eventually "blow up",

[1] In French: Cependant tout ce que la Théorie des fluides renferme, est contenu dans les deux équations rapportées cy-dessus, de sorte que ce ne sont pas les principes de Méchanique qui nous manquent dans la poursuite de ces recherches, mais uniquement l'Analyse, qui n'est pas encore assés cultivée, pour ce dessein: et partant on voit clairement, quelles découvertes nous restent encore à faire dans cette Science, avant que nous puissions arriver à une Théorie plus parfaite du mouvement des fluides.

* Corresponding author. Tel.: +33 4 92003035; fax: +33 4 92003058.
E-mail address: uriel@obs-nice.fr (U. Frisch).

0167-2789/$ - see front matter © 2006 Elsevier B.V. All rights reserved.
doi:10.1016/j.physd.2006.05.011

that is become singular in a finite time (see, e.g. Refs. [3,4])? In two dimensions it has been known since the 1930's that flow in a bounded domain, initially sufficiently smooth, never blows up [5,6]. It was also shown that if such a 2D flow is initially analytic it will stay so forever [7–9]. However, in the course of time, such flow can develop very fine scales and there is a large discrepancy between the analytic estimation of how the smallest scale decreases in time (a double exponential) and what is found in numerical simulations (a simple exponential; see, e.g., Ref. [10]).

The likely cause of the discrepancy is *depletion*, the phenomenon by which high-Reynolds number or inviscid incompressible flow tends to organize itself into structures having vastly reduced nonlinearities (see, e.g., Ref. [11]). Depletion, which is still very poorly understood, may hold the key for understanding why 3D high-Reynolds number flow seems never to blow up, at least in simulations.[2] In this paper we shall focus on the two-dimensional case.

There are well-known 2D examples of depletion, such as flows which depend only on one Cartesian coordinate or on the radial polar coordinate. Such flows are however steady and thus globally depleted, with no dynamics. In this paper we shall be interested in 2D flow with an initial stream function which is a real trigonometric polynomial in the space variables, of the sort already considered in Refs. [4,12]. These are the 2D counterparts of well-known 3D flows such as Taylor–Green and Kida–Pelz [13–17] which have been used for (so far inconclusive) investigation of finite-time blow-up. Our 2D flows have generally non-trivial dynamics and display locally very strong depletion.

Trigonometric polynomials are instances of entire functions, that is, functions which are analytic in the whole complex domain. The only singularities of such functions are at complex infinity. The solution of the Euler equations at times $t > 0$ sufficiently small can then be extended analytically into the complex domain [7–9]. There is strong numerical evidence in 2D and also in 3D that such flow does not stay entire and develops singularities at certain complex locations for any $t > 0$ [10,14,4,12]. Complex singularities are usually detected through the Fourier transforms of the solution: roughly, there is an exponential tail related to the distance of the nearest singularity from the real domain, accompanied by an algebraic prefactor related to the nature (also called type or structure) of the singularities.

Little is known about the nature of complex singularities of the Euler equations. In Refs. [4] and [12] it is shown numerically for the 2D case with the initial stream function $\cos x_1 + \cos 2x_2$ that the complex singularities lie on a smooth manifold and that the vorticity becomes infinite when approaching the singular manifold; there is however considerable uncertainty as to the scaling law of this divergence. In Ref. [18] the motion of preexisting complex-space singularities is studied analytically but their nature is kept quite arbitrary. In Ref. [19] traveling-wave solutions with a pure imaginary velocity are studied for 3D axisymmetrical flow with swirl; using an ultra-high precision[3] numerical method, the singularities in the complexified axial variable are mapped out as a function of the (real) radial variable and found to lie on a smooth curve; the nature of the singularities is obtained using a "sliding fit" method. In Ref. [20], for the vortex sheet problem with an initially analytic interface, the nature of complex singularities of the interface is obtained using an ultra-high precision method and a "pointwise fit". The sliding fit and the pointwise fit are very closely related to the method we use in Section 3.1 and we shall come back to this matter. Since the work of Krasny [21], it appears that ultra-high precision is a prerequisite for obtaining numerical information on the nature of singularities, particularly when they are in the complex domain.

From a *theoretical* point of view, for many nonlinear equations of mathematical physics a very successful tool in studying the nature of singularities has been dominant balance and its refined versions such as Painlevé analysis [22]. Dominant balance analysis typically gives *universal* singularities, that is singularities whose positions may depend on the initial conditions but their nature does not. The simplest instance is the 1D viscous Burgers equation whose complex-space singularities are simple poles, obtainable by balancing the nonlinear term against the viscous one. For the d-dimensional incompressible Euler equations, attempts to use dominant balance fail because of the particular structure of the nonlinearity: if we assume that the solution becomes singular on a complex manifold of dimension $d - 1$, the nonlinearity vanishes to leading order. This is just a consequence of the simplest form of depletion, the vanishing of nonlinearity for solutions which depend on a single spatial coordinate. The nature of singularities cannot be obtained by a dominant balance argument; actually, as we shall see, complex singularities of the 2D Euler equation display a very unusual *non-universality*.

In this paper we will mainly discuss the *short-time asymptotic régime* presented in Ref. [4] and extensively used in Ref. [12] which gives us the most accurate information on the nature of complex singularities.[4] After briefly introducing it in Section 2 we will show that this régime can be reformulated as a "pseudo-hydrodynamic" Euler problem, in which all the action including the singularities takes place in a plane extending in the pure imaginary directions, but our usual hydrodynamic intuition is still applicable. The short-time asymptotics allows us to obtain recurrence relations for spatial Fourier components involving only wavectors $\boldsymbol{k} = (k_1, k_2)$ with $k_1 \geq 0$ and $k_2 \geq 0$, a feature which is also present in the Moore approximation for vortex sheets [23] and its generalization to smooth flow [19]; as a consequence Fourier components can be calculated in ultra-high precision without any truncation error. In Section 3 we present the numerical evidence for simple scaling laws

[2] For the case of 3D inviscid Euler flow there is no truly conclusive evidence in favor of blow-up [4,17]. Furthermore, if the flow is initially analytic, any real singularity will have to be preceded by complex-space singularities [8,9].

[3] That is, higher than double precision.

[4] Henceforth, Ref. [12] will be cited as MBF.

associated to complex singularities and determine the nature of the singularities with high precision. Analyzing short-time asymptotics for different initial conditions, we find that the singularities are non-universal. In Section 4 we describe the global and local geometry of the pseudo-hydrodynamic flow, including depletion of nonlinearity which is especially strong near the singularities.

Sections 3 and 4 both involve a mixture of numerical results and of theoretical arguments, some heuristic, some more rigorous. We must stress that at the moment we do understand various features of the solution, in particular why the scaling exponent for singularities does not depend on the direction, but we failed so far to reproduce by theory the non-universal scaling exponents observed for the singularities. Nevertheless by moving to yet another level of toy-modeling (the equivalent for our problem of considering the vorticity as a passive scalar in a prescribed velocity field), we can determine the nature of the corresponding complex singularities using dynamical systems tools (Section 5). The nature of these "advection" singularities is however universal and therefore does not reproduce an essential feature of the nonlinear Euler flow. Finally, conclusions, open problems and a tentative road map for future research on blow-up are presented in Section 6. To make the present paper reasonably self-contained we shall occasionally re-derive results already found in Ref. [4] and MBF.

2. Short-time asymptotics and pseudo-hydrodynamics

We are interested in the short-time asymptotics for the 2D Euler equation, written in terms of the stream function

$$\partial_t \nabla^2 \Psi(\boldsymbol{x}, t) - J(\Psi, \nabla^2 \Psi) = 0, \tag{1}$$

where $\boldsymbol{x} = (x_1, x_2)$ and $J(f, g) \equiv \partial_1 f \partial_2 g - \partial_1 g \partial_2 f$. The initial condition $\Psi_0(\boldsymbol{x}) \equiv \Psi(\boldsymbol{x}, 0)$ is a real 2π-periodic trigonometric polynomial of the form $\Psi_0(\boldsymbol{x}) = \sum_{\boldsymbol{k}} \hat{F}^{(0)}(\boldsymbol{k})\, \mathrm{e}^{\mathrm{i}\boldsymbol{k}\cdot\boldsymbol{x}}$, where the sum has only a finite number of terms. Here $\boldsymbol{k} = (k_1, k_2)$, where k_1 and k_2 are signed integers. The short-time asymptotics is simplest when the initial condition has only two orthogonal Fourier modes, as in Refs. [4,12] where the assumed initial condition is

$$\Psi_0(\boldsymbol{x}) = \cos x_1 + \cos 2x_2. \tag{2}$$

In what follows we shall call this initial condition the Standard Orthogonal Case (SOC). One of our present goals is to investigate to what extent complex singularities are or are not universal; we are thus naturally led to considering more general cases, having, for example, more than two modes in the initial conditions. In the Appendix it will be shown that the short-time asymptotic régime for the multimode case can be reduced to a set of two-mode initial conditions. We may thus without loss of generality limit ourselves to two-mode initial conditions of the form

$$\Psi_0(\boldsymbol{x}) = h_1\, \mathrm{e}^{\mathrm{i}\,\mathfrak{p}\cdot\boldsymbol{x}} + h_2\, \mathrm{e}^{\mathrm{i}\,\mathfrak{q}\cdot\boldsymbol{x}} + \text{c.c.} \tag{3}$$

Here c.c. stands for "complex conjugate", $\mathfrak{p} = (\mathfrak{p}_1, \mathfrak{p}_2)$ and $\mathfrak{q} = (\mathfrak{q}_1, \mathfrak{q}_2)$ are two vectors with signed integer components. Furthermore, we assume that $\mathfrak{p}$ and $\mathfrak{q}$ are not parallel and do not have the same modulus since otherwise the two-mode initial condition is a time-independent solution of the Euler equation. By performing if needed a suitable translation, we can then assume that h_1 and h_2 are positive. Finally, since our goal here is primarily to demonstrate non-universality of the nature of the singularities with respect to the initial conditions, we shall not strive for the greatest generality and limit ourselves to *basic modes* with non-negative components such that $\mathfrak{p}_1\mathfrak{q}_2 - \mathfrak{q}_1\mathfrak{p}_2 > 0$.

Eq. (1) has a solution in the form of a Taylor series in the time variable

$$\Psi(\boldsymbol{x}, t) = \sum_{n\geq 0} \Psi_n(\boldsymbol{x})\, t^n, \tag{4}$$

where Ψ_0 is the initial condition and the $\Psi_n(\boldsymbol{x})$'s for $n \geq 1$ are easily shown to satisfy the recursion relations:

$$\nabla^2 \Psi_{n+1} = \frac{1}{n+1} \sum_{m+p=n} J(\Psi_m, \nabla^2 \Psi_p). \tag{5}$$

For the two-mode initial condition (2) all the $\Psi_n(\boldsymbol{x})$ are trigonometric polynomials that can be continued analytically to complex locations $\boldsymbol{z} = \boldsymbol{x} + \mathrm{i}\,\boldsymbol{y}$. Since the initial condition has its singularities at infinity, we expect, by continuity, that at short times the singularities will have large imaginary parts $|y_1|$ and $|y_2|$. Let us now suppose that $y_1 \to +\infty$ and $y_2 \to +\infty$ in such a way that their ratio y_2/y_1 stays finite but arbitrary. Obviously, the four vectors $(\mathfrak{p}_1, \mathfrak{p}_2)$, $(-\mathfrak{p}_1, -\mathfrak{p}_2)$, $(\mathfrak{q}_1, \mathfrak{q}_2)$ and $(-\mathfrak{q}_1, -\mathfrak{q}_2)$ divide the $\boldsymbol{k}$-space into four angular sectors so that, for example, in the first angular sector $\mathfrak{p}_2/\mathfrak{p}_1 \leq y_2/y_1 \leq \mathfrak{q}_2/\mathfrak{q}_1$. Then, for $\boldsymbol{z}$ such that $\boldsymbol{y}$ lies in the first angular sector, to leading order any additional factor t in the expansion (4) is accompanied by either a factor $\mathrm{e}^{-i\,\mathfrak{p}\cdot\boldsymbol{z}}$ or a factor $\mathrm{e}^{-i\,\mathfrak{q}\cdot\boldsymbol{z}}$, thus giving amplitude factors $t\mathrm{e}^{\mathfrak{p}\cdot\boldsymbol{y}}$ and $t\mathrm{e}^{\mathfrak{q}\cdot\boldsymbol{y}}$, respectively. When $t \to 0$ and $|\boldsymbol{y}| \to \infty$ these factors remain finite, provided $\mathfrak{p}\cdot\boldsymbol{y}$ and $\mathfrak{q}\cdot\boldsymbol{y}$ are shifted by $\ln t$. This suggests that the short-time asymptotics is obtained by the *similarity ansatz*

$$\Psi(z, t) = (1/t) F(\tilde{\boldsymbol{z}}), \tag{6}$$

$$\tilde{\boldsymbol{z}} = (\tilde{z}_1,\ \tilde{z}_2) \equiv (z_1 + \mathrm{i}\,\lambda_1 \ln t,\ z_2 + \mathrm{i}\,\lambda_2 \ln t), \tag{7}$$

where λ_1 and λ_2 are determined by

$$\lambda_1 = \frac{\mathfrak{p}_2 - \mathfrak{q}_2}{\mathfrak{q}_1\mathfrak{p}_2 - \mathfrak{q}_2\mathfrak{p}_1} \quad \text{and} \quad \lambda_2 = \frac{\mathfrak{q}_1 - \mathfrak{p}_1}{\mathfrak{q}_1\mathfrak{p}_2 - \mathfrak{q}_2\mathfrak{p}_1}. \tag{8}$$

Substitution in (1) gives the *similarity equation*

$$\tilde{\nabla}^2(-1 + \mathrm{i}\,\lambda_1 \tilde{\partial}_{z_1} + \mathrm{i}\,\lambda_2 \tilde{\partial}_{z_2}) F = \tilde{J}(F, \tilde{\nabla}^2 F), \tag{9}$$

where the tilde means that the partial derivatives are taken with respect to the new variables. The initial condition (2) becomes an asymptotic boundary condition

$$F(\tilde{\boldsymbol{z}}) \simeq h_1 \mathrm{e}^{-\mathrm{i}\,\mathfrak{p}\cdot\tilde{\boldsymbol{z}}} + h_2 \mathrm{e}^{-\mathrm{i}\,\mathfrak{q}\cdot\tilde{\boldsymbol{z}}}, \quad \tilde{y}_1 \to -\infty, \tilde{y}_2 \to -\infty. \tag{10}$$

In (9) the second and third terms on the l.h.s. can be viewed as stemming from the advection by a pure imaginary constant "drift velocity". This is because we are following

the singularities coming "down" from complex infinity. It is important to observe that (9) is an exact consequence of the Euler equation. The only place where an approximation is made is in the boundary condition (10) where harmonics containing for example $e^{+i\,\mathbf{p}\cdot\tilde{\mathbf{z}}}$ and $e^{+i\,\mathbf{q}\bar{\tilde{z}}}$ are discarded because such terms are exponentially subdominant at short times.

In what follows we shall generally limit ourselves to the SOC, giving occasionally an indication of what is valid for more general two-mode cases. The general case can easily be handled but we wish to avoid burdening the reader with unnecessarily complicated statements and equations.

The function $F(\tilde{z})$, which is 2π-periodic in $\tilde{x}_1$ and π-periodic in $\tilde{x}_2$, is analytic in the product of the half-spaces $\tilde{y}_1 \le 0$ and $\tilde{y}_2 \le 0$ and thus its spatial Fourier series has only harmonics of the form $e^{-i\,(k_1\tilde{z}_1+k_2\tilde{z}_2)}$ with $k_1 \ge 0$ and $k_2 \ge 0$. Its Fourier series is here written as[5]

$$F(\tilde{z}_1,\tilde{z}_2) = \sum_{k_1=0}^{\infty}\sum_{k_2=0}^{\infty}(-1)^{k_1}\hat{F}(k_1,k_2)e^{-i\,k_1\tilde{z}_1}e^{-i\,k_2\tilde{z}_2}. \tag{11}$$

The reason for the presence of the factor $(-1)^{k_1}$ will become clear shortly. The Fourier coefficients $\hat{F}(\boldsymbol{k}) \equiv \hat{F}(k_1,k_2)$ can be calculated recursively from the relation given in MBF which follows from (9)

$$\hat{F}(k_1,k_2) = -\frac{1}{k_1+k_2/2-1}\,\frac{1}{|\mathbf{k}|^2} \times \sum_{p_1=0}^{k_1}\sum_{p_2=0}^{k_2}(\mathbf{p}\wedge\mathbf{k})|\mathbf{k}-\mathbf{p}|^2\hat{F}(p_1,p_2)\hat{F}(k_1-p_1,k_2-p_2). \tag{12}$$

Here, $\mathbf{p}\wedge\mathbf{k} \equiv p_1k_2 - p_2k_1$. Because there are no Fourier harmonics with negative k_1 or k_2, the convolutions in (12) only involve positive arguments. This feature, which allows truncation-free determination of Fourier coefficients, is also present in the Moore approximation for the vortex sheet problem and in its generalization to axisymmetrical flow [19, 23]. The initialization of the recursion relations requires the knowledge of the coefficients along the "edges", that is the half-lines $k_1 = 0$ and $k_2 = 0$. In the present case $\hat{F}(0,2) = 1/2$ and $\hat{F}(1,0) = -1/2$ while all the other edge harmonics are zero.[6] It has been shown in MBF that, with the choice made above in (11), the coefficient $\hat{F}(1,0)$ is the only one that is negative. All the other ones are non-negative. This result has so far only been established by (very solid) numerical computations and holds for all the two-mode initial conditions studied. As we shall see, this has important consequences for the geometry of singularities.

We shall now show that (9) can be reformulated as the steady solution of a *pseudo-hydrodynamic* problem in a suitable imaginary plane. Since we are working with analytic functions, we can replace the complex partial derivatives $\tilde{\partial}_{z_1}$ and $\tilde{\partial}_{z_2}$ by $-i\,\tilde{\partial}_{y_1}$ and $-i\,\tilde{\partial}_{y_2}$, holding the x-coordinates fixed. In terms of such y-derivatives (9) becomes an equation with real coefficients. If we furthermore choose x_1 and x_2 such that the boundary condition (10) becomes real then the solution "above such points" F is also real. This happens for $x_1 = 0, \pi$ and for $x_2 = 0, \pi/2, \pi, 3\pi/2$. The positivity of all but one of the Fourier coefficients defined in (11) with the factor $(-1)^{k_1}$ amounts to stating that, after moving the origin to $(\pi, 0)$, all but one of the usual Fourier coefficients of F are positive. As we shall see in Section 4, this gives us the possibility of analyzing the (short-time) complex singularities by focusing solely on the y-plane above $(\pi, 0)$. This point turns out also to be a center of symmetry for the Euler flow with the initial condition (2), but it is not clear whether this matters.[7] Henceforth we shall consider the y-plane above $(\pi, 0)$.

We define a pseudo-stream function in terms of the y-coordinates (from now on we drop the tilde on the y variables for notational simplicity)

$$\psi(\mathbf{y}) = \psi(y_1,y_2) \equiv \frac{1}{2}y_1 - y_2 + F(\pi + i\,y_1, i\,y_2), \tag{13}$$

$$= \frac{1}{2}y_1 - y_2 + \sum_{\boldsymbol{k}}\hat{F}(\boldsymbol{k})\,e^{\boldsymbol{k}\cdot\boldsymbol{y}}, \tag{14}$$

where the two linear terms on the r.h.s. have been introduced to avoid having an additional advection term. Note that because of these terms, ψ is not the continuation to complex coordinates of a function periodic in x_1 and x_2.

It is now elementary to check that (9) and (10) are equivalent to taking the steady-state (τ-independent) solution of the pseudo-hydrodynamic equation

$$\partial_\tau\nabla^2\psi - J(\psi,\nabla^2\psi) = -\nabla^2\psi, \tag{15}$$

with the asymptotic boundary condition (for $y_1,\ y_2 \to -\infty$)

$$\psi(y_1,y_2) - \frac{1}{2}y_1 + y_2 \simeq -\frac{1}{2}e^{y_1} + \frac{1}{2}e^{2y_2}. \tag{16}$$

Here, in order to bring out familiar hydrodynamic notation, we have introduced a pseudo-time variable τ.[8] We are using $\nabla = (\partial_1,\ \partial_2)$ for ∇_y and the Jacobian J has its usual definition in terms of y-derivatives. We now introduce a pseudo-velocity and a pseudo-vorticity by the usual definitions[9]:

$$\boldsymbol{v} = (v_1,v_2) \equiv (\partial_2\psi, -\partial_1\psi) \tag{17}$$

$$= -(1,1/2) + \sum_{\boldsymbol{k}}(k_2,-k_1)\,\hat{F}(\boldsymbol{k})\,e^{\boldsymbol{k}\cdot\boldsymbol{y}}, \tag{18}$$

$$\omega \equiv -\nabla^2\psi, \tag{19}$$

$$= \sum_{\boldsymbol{k}} -k^2\,\hat{F}(\boldsymbol{k})\,e^{\boldsymbol{k}\cdot\boldsymbol{y}}, \tag{20}$$

[5] In MBF k_1 and k_2 were defined with the opposite sign.

[6] In the general case of two basic modes $\mathbf{p}$ and $\mathbf{q}$, the main change with respect to the SOC is the replacement in (12) of the denominator $k_1 + k_2/2 - 1$ by $\lambda_1k_1 + \lambda_2k_2 - 1$, where λ_1 and λ_2 are defined in (8).

[7] Note that streamlines have a hyperbolic structure near $(\pi, 0)$, but an elliptic structure near $(0, 0)$ which is also a center of symmetry.

[8] If we allow the function F and thus ψ to also depend on t and set $\tau = \ln(1/t)$, we obtain precisely (15).

[9] The true velocity is actually pure imaginary in the y-plane and the true vorticity is $-\omega$.

in terms of which (15) reads

$$[\partial_\tau \omega] + \boldsymbol{v} \cdot \nabla \omega + \omega = 0, \tag{21}$$

with the boundary conditions (for $y_1,\ y_2 \to -\infty$)

$$\boldsymbol{v} \simeq \left(-1,\ -\frac{1}{2}\right), \quad \omega \simeq \frac{1}{2}\mathrm{e}^{y_1} - 2\mathrm{e}^{2y_2}. \tag{22}$$

For other initial conditions, only the boundary condition (22) must be modified. The τ-derivative term has been put within square brackets since we are only interested in the steady-state solution. Note that the pseudo-hydrodynamic formulation in the y-plane is that of a quasi-two-dimensional flow in a 3D container with bottom friction producing a Rayleigh drag. In this formulation $\tau \to +\infty$ as we approach the initial instant. An alternative interpretation is to define τ as $\ln t$, to avoid reversing the course of time, and then to change the signs of $\boldsymbol{v}$ and of ω and replace the Rayleigh drag by an instability.

In the pseudo-hydrodynamic formulation it is now obvious that the problem is invariant under an arbitrary translation $\boldsymbol{h} = (h_1,\ h_2)$ in y-space. By (14), such a translation amounts to a factor $\mathrm{e}^{\boldsymbol{k}\cdot\boldsymbol{h}}$ on the Fourier coefficients $\hat{F}(\boldsymbol{k})$. It follows, as noted in MBF, that the set of initial conditions $\Psi_0(\boldsymbol{x}) = \mathrm{e}^{h_1}\cos x_1 + \mathrm{e}^{2h_2}\cos 2x_2$ is equivalent to the SOC as long as $\boldsymbol{h}$ is within the analyticity domain. Similarly, a translation in k-space with integer components $(n_1,\ n_2)$ is equivalent to multiplying $F(\pi + \mathrm{i}\, y_1,\ \mathrm{i}\, y_2)$ by the exponential factor $\mathrm{e}^{n_1 y_1 + n_2 y_2}$ in y-space. The exponential being an entire function, this changes neither the positions nor the nature of the singularities at finite distance.

3. Numerical investigation of scaling laws in Fourier space

We shall show in this section that the solution of the Euler equation in the short-time asymptotic régime defined in the previous section has remarkably clean scaling properties in Fourier space. By this we mean that the wavenumber dependence of the Fourier coefficients is represented as a decreasing exponential multiplied by an algebraic prefactor whose exponent can be measured very accurately. Such a functional form is not surprising. In fact the exponential is the signature of the location of a singularity while the prefactor encodes the nature of the singularity. For one-dimensional analytical functions with isolated singularities in the complex space this is well known: a singularity at $z_\star$ of the form $(z - z_\star)^\rho$ has a signature in the modulus of the Fourier transorm at high wavenumbers k of the form $C|k|^{-\rho-1}\mathrm{e}^{-\delta|k|}$, where δ is the distance of $z_\star$ to the real axis (see, e.g., Ref. [24]). Such asymptotic results have been extended in the 1990's to the Fourier transforms of periodic analytical functions of several complex variables when the wavevector $\boldsymbol{k}$ tends to infinity with a fixed rational slope $\tan\theta = k_2/k_1 = p/q$, where p and q are relative prime integers [25–27].

When the Fourier coefficients are obtained numerically, there is a maximum wavenumber $k_{\max}$. Unless it is taken very large, there will be very few points on the line of slope p/q as soon as q is not a very small integer. But a large value of $k_{\max}$ entails extremely small Fourier coefficients because of the exponential decrease with the wavenumber. Thus, as stressed in MBF, very high precision may be needed to avoid swamping by the rounding errors. Truncation errors are not an issue in the short-time asymptotic régime since the Fourier coefficients can be calculated from (12) with arbitrary accuracy.

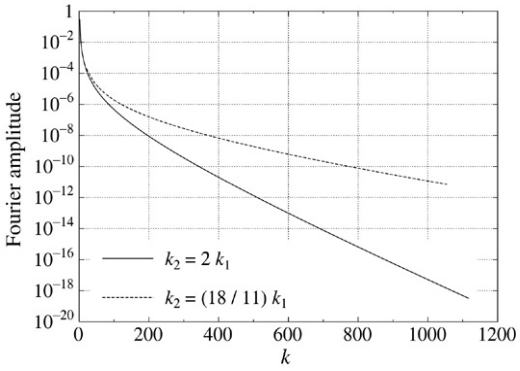

Fig. 1. Fourier coefficients of the stream function F along two lines of different slopes as a function of $k \equiv |\boldsymbol{k}|$ in lin–log coordinates.

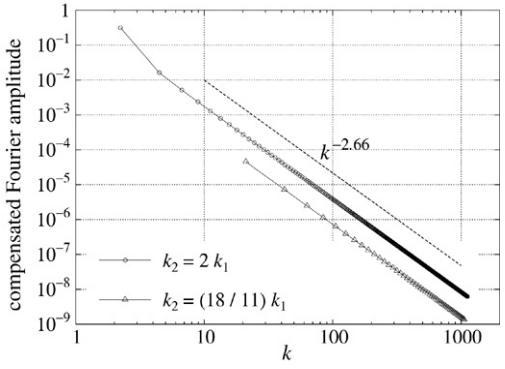

Fig. 2. Same as in Fig. 1 after division by $\exp(-\delta k)$ (compensated Fourier coefficients) in log–log coordinates. Most of the points are in the asymptotic power-law régime, at least visually.

The data obtained for the SOC initial condition in MBF had wavenumbers $k \equiv |\boldsymbol{k}|$ up to 1000 or 2000, depending on the direction and were calculated with 35-digit accuracy.[10] Most of the results presented here are based on the 35-digit calculation. Additional calculations are also presented here with various initial conditions, with up to 100-digit precision and wavenumbers which can reach 4000 in particular directions. We note that the MPFUN90 package for high-precision calculation used in MBF, here and in Ref. [19] makes use of fast Fourier transform techniques. Thus the CPU time per multiplication, as a function of the number of digits N, is proportional to $N \log N$ [28].

We now show that it is quite easy in principle to observe scaling by analyzing the behavior of the Fourier coefficients in directions of rational slope. Figs. 1 and 2 give two examples of the analysis of Fourier coefficients along straight lines through

[10] In MBF it was stated that, when using only double-precision (15-digit) accuracy, unacceptably large errors are obtained beyond wavenumber 800. Actually, as pointed out by Zimmermann (private communication), the double-precision calculation can be modified in such a way that, up to wavenumber 1000, the relative error on Fourier modes does not exceed 10^{-5}.

the origin[11] in a direction of rational slope, using the data from MBF for the Fourier coefficients of the stream function with SOC initial conditions. The first case has $k_2/k_1 = 2$, the direction with the largest number of grid points having non-vanishing Fourier coefficients. The second case has $k_2/k_1 = 18/11$, the direction with the slowest decrease of the Fourier coefficients. Fig. 1, which shows the Fourier coefficients in lin–log coordinates, reveals an exponential tail $\propto \mathrm{e}^{-\delta k}$; a least square fit gives $\delta = 0.021$ for the first case and $\delta = 0.0065$ for the second case.[12] In Fig. 2 we show the "compensated" Fourier coefficients obtained by dividing by the exponential term; the result is then represented in log–log coordinates in order to look for an algebraic prefactor $\propto k^{-\alpha}$. The quality of the scaling obtained is impressive: over most of the range we cannot on a log–log plot visually distinguish the prefactor from a power law with exponent $\alpha = 8/3$. As we shall see, the exponent does not depend on the direction chosen.

3.1. Technique for capturing algebraic prefactors

Determining the scaling properties as done above by use of least square fits, compensating exponentials and log–log plots is not optimally adapted for delicate issues such as studying the dependence of the prefactor exponent on the direction of the wavector or on the initial conditions. As pointed out by Shelley [20], it is better to remove some of the subjective biases present in a least square fit (such as choosing the range in k). We shall make use of his method of point-wise fit (also used in Ref. [19], where it is called a sliding fit), followed by an extrapolation step as now explained.

In $\boldsymbol{k}$-space, a direction of rational positive slope is characterized by $k_2/k_1 = \tan\theta = q/p$ (where the positive integers p and q are taken to be relative primes). All the $\boldsymbol{k}$ vectors on the line of slope p/q through the origin are thus of the form $\boldsymbol{k} = n\boldsymbol{k}_0$, where $\boldsymbol{k}_0 \equiv (p, q)$ and n is a positive integer. What we have seen at the beginning of Section 3 suggests that for a given direction of rational slope $\tan\theta$, the Fourier coefficients of the stream function can be represented, for sufficiently large k, as

$$\hat{F} \simeq C(\theta) k^{-\alpha(\theta)} \mathrm{e}^{-\delta(\theta)k}. \tag{23}$$

Henceforth α, C and δ will be referred to as the prefactor exponent, the constant and the decrement, respectively. When there is no ambiguity, the θ-dependence will be omitted. Following Ref. [20], let us assume for a moment that (23) holds exactly and let us set $\hat{F}_n(\boldsymbol{k}_0) \equiv \hat{F}(n\boldsymbol{k}_0)$. It then follows that if we know $\hat{F}_n(\boldsymbol{k}_0)$ for any three consecutive values, say $n-1$, n and $n+1$, we can determine C, α and δ by

$$\alpha = \frac{\ln\left(\frac{\hat{F}_{n-1}(\boldsymbol{k}_0)\hat{F}_{n+1}(\boldsymbol{k}_0)}{\hat{F}_n^2(\boldsymbol{k}_0)}\right)}{\ln\left(\frac{n^2}{(n-1)(n+1)}\right)}, \tag{24}$$

[11] All the lattice lines of a given rational slope have the same high-k asymptotics, due to the observation made at the end of Section 2.

[12] Why the minimum value is so small is a matter we shall come back to in Section 5.

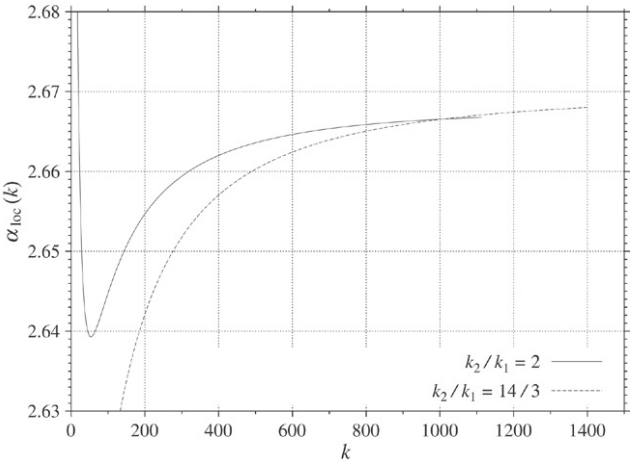

Fig. 3. Local prefactor exponent $\alpha_{\mathrm{loc}}(k)$ versus wavenumber for two values of the slope.

$$\delta = \frac{1}{|\boldsymbol{k}_0|}\left[\ln\left(\frac{\hat{F}_n(\boldsymbol{k}_0)}{\hat{F}_{n+1}(\boldsymbol{k}_0)}\right) + \alpha \ln\left(\frac{n}{n+1}\right)\right], \tag{25}$$

$$\ln C = \ln \hat{F}_n(\boldsymbol{k}_0) + \alpha \ln[(n)|\boldsymbol{k}_0|] + n|\boldsymbol{k}_0|\delta. \tag{26}$$

The expression (24) for α follows immediately by noticing that in the combination $\hat{F}_{n-1}\hat{F}_{n+1}/\hat{F}_n^2$ the constant C and the exponential factor both drop out. The other two expressions are readily established by taking the logarithm of (23).

Of course, we have no reason to expect that (23) holds *exactly* for arbitrary wavenumbers. At best it will hold asymptotically at large wavenumbers. Nevertheless we can use (25) *and* (26) to calculate a *local prefactor exponent* $\alpha_{\mathrm{loc}}(k)$, which depends on the wavenumber. Here we have chosen to use as arguments of the local quantities the wavenumber $k = n|\boldsymbol{k}_0|$.

The typical behavior of $\alpha_{\mathrm{loc}}(k)$ is shown in Fig. 3 for two directions. For large values of k the curves grow to an asymptotic value close to 8/3. Globally, $\alpha_{\mathrm{loc}}(k)$ is found to be non-monotonic when $\theta < \theta_\star$ with $\tan\theta_\star$ close to 3 (but not very sharply defined) and monotonic above $\theta_\star$.

To estimate the asymptotic value α_∞ we must *extrapolate* the data beyond the largest available wavenumber at which they are known with acceptable accuracy. Since the only causes of error in $\alpha_{\mathrm{loc}}(k)$ are rounding errors, we can measure such errors by comparing runs having different levels of precision. Fig. 4 shows the discrepancy (absolute error) of $\alpha_{\mathrm{loc}}(k)$ obtained with 15- and 35-digit precision. The error is seen to grow with the wavenumber in an approximately exponential fashion, the highest value being about 10^{-8} around wavenumber 1000. We shall see that the error involved in the extrapolation may be much larger than 10^{-8}.

One well-known difficulty with extrapolation is that the problem may not be well-posed unless one has additional information on the functional form of the convergence to zero of the remainder $\alpha_\infty - \alpha_{\mathrm{loc}}(k)$. In Ref. [20], which deals with the shape of a vortex sheet continued analytically to complex parameters, it is assumed that branch singularities of unknown exponent are present and that the high-k behavior of the one-dimensional Fourier transform can be obtained from Laplace's

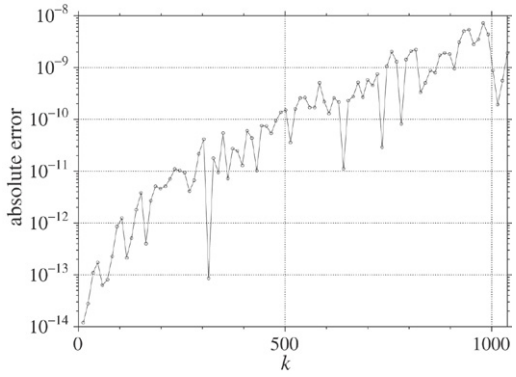

Fig. 4. Discrepancy between 15- and 35-digit calculation of the local prefactor exponent $\alpha_{\rm loc}(k)$ along $k_2/k_1 = 5/3$, as an estimate of the absolute error on $\alpha_{\rm loc}$.

method to leading and first subleading orders; the inclusion of the first subleading correction allows a much improved determination of the exponent. This extrapolation procedure is equivalent to assuming that the remainder $\alpha_\infty - \alpha_{\rm loc}(k)$ goes to zero as $1/k$. For our problem, unfortunately no simple functional form of the remainder, such as algebraic, exponential or inverse logarithmic decrease, gives a satisfactory fit. An efficient extrapolation method for a wide range of functional behaviors of the remainder is the *epsilon algorithm* of Wynn [29], related to the Shanks transform method [30]. It is an algorithm for acceleration of convergence of a sequence $S = (s^{(0)}, s^{(1)}, s^{(2)}, \ldots, s^{(i)}) \in \mathbb{C}$, and it comprises the following initialization and iterative phases.

Initialization: For $n = 0, 1, 2, \ldots$

$$\varepsilon_{-1}^{(n)} = 0 \quad \text{(artificially)}, \quad \varepsilon_0^{(n)} = s^{(n)}. \tag{27}$$

Iteration: For $n = 0, 1, 2, \ldots$

$$\varepsilon_{l+1}^{(n)} = \varepsilon_{l-1}^{(n+1)} + [\varepsilon_l^{(n+1)} - \varepsilon_l^{(n)}]^{-1}. \tag{28}$$

After a few iterations of the algorithm, applied to 35-digit SOC data, the $\varepsilon_l^{(n)}$'s with even l become almost constant and give an estimate of the *extrapolated exponents* (see Fig. 5). The epsilon-algorithm extrapolated exponents will be used when discussing results (unless otherwise stated). We have also used the recently introduced asymptotic interpolation method of van der Hoeven [31] which strips off successively leading and subleading terms by suitable transformations before doing the interpolation. This method works impressively for the passive scalar model discussed in Section 5 for which both leading and subleading terms in the high-k expansion can be determined from numerical data. In the nonlinear case, the asymptotic interpolation method gives exponents consistent with those determined by the epsilon algorithm with a relative error of about 10^{-3}; we have so far not been able to determine numerically the functional form of subleading corrections. As we shall see in Section 4.3, theory tells us that α should not depend on the angle θ. We suspect that θ-dependent subleading corrections account for the slight apparent variation of α with θ, reported in Section 3.2.

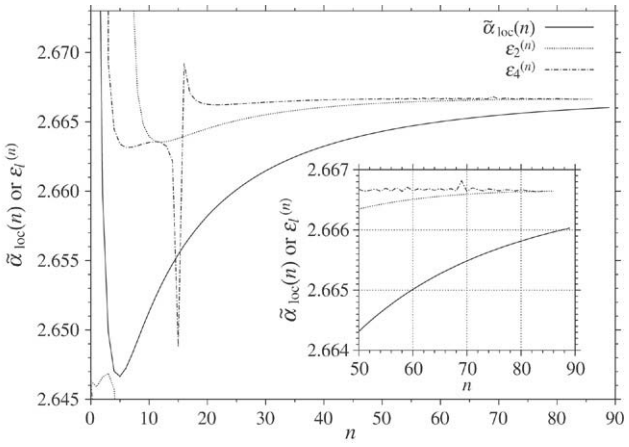

Fig. 5. Local prefactor exponent $\tilde{\alpha}_{\rm loc}(n)$ for the nth point along the line $k_2/k_1 = 5/3$ which has $(k_1, k_2) = (5n, 3n)$; it is shown together with its second- and fourth-order epsilon-algorithm extrapolated values. Inset: enlargement for $n > 50$.

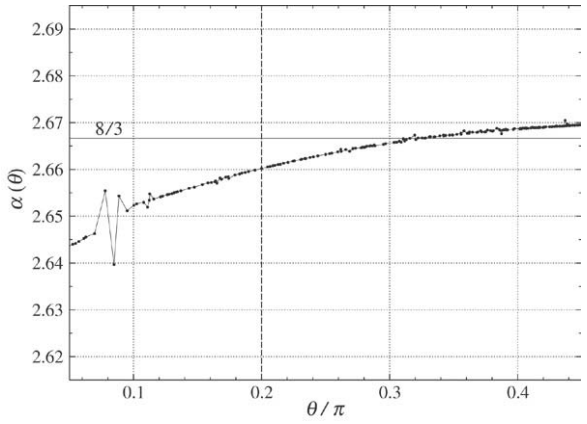

Fig. 6. Angular dependence of the prefactor exponent $\alpha(\theta)$ for the SOC (extrapolated by the epsilon algorithm). Below $\theta = 0.2\pi$ (long dashed line) the extrapolation cannot be trusted.

3.2. Results for the SOC

For the SOC, whose initial stream function is $\cos x_1 + \cos 2x_2$, we now use the method described in Section 3.1 to calculate the prefactor exponent $\alpha(\theta)$, the decrement $\delta(\theta)$ and the constant $C(\theta)$.

Figs. 6–8 show the angular variation of α, δ and C, respectively, excluding near-edge ranges where θ is close to 0 or $\pi/2$ which deserve separate discussion (see Section 3.4).

The most striking result is the very weak angular dependence of the prefactor exponent, which over the range $0.2\pi < \theta < 0.45\pi$ is given by $\alpha = 2.66 \pm 0.01$, consistent with the theory which predicts independence on θ (Section 4.3). This immediately leads to asking if $\alpha_{\rm SOC} = 8/3$. The short answer is: we do not know. We shall come back to this at length.

The angular dependence of δ has already been reported in MBF where it was measured by decomposing the set of directions into small angular sectors.[13] We find that $\delta(\theta)$

[13] In MBF θ was varying in the third quadrant; here, because of the aforementioned change of notation θ varies in the first quadrant. Furthermore,

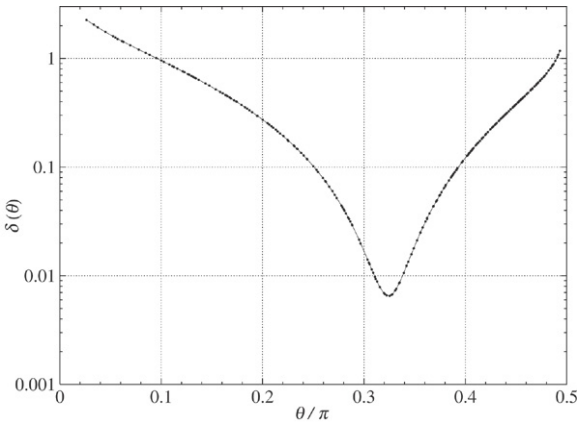

Fig. 7. Angular dependence of the decrement $\delta(\theta)$ for SOC.

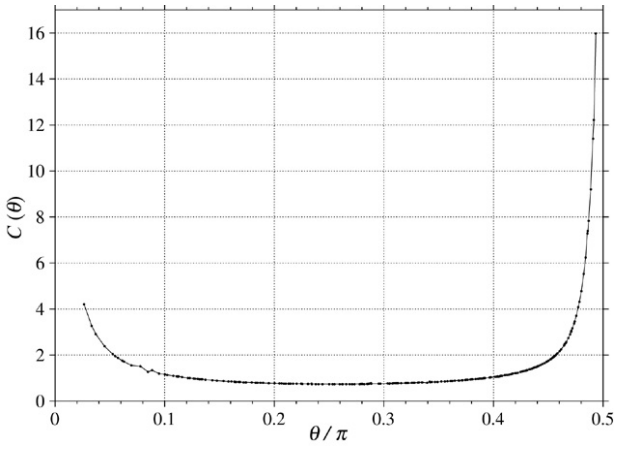

Fig. 8. Angular dependence of the constant $C(\theta)$ for SOC.

achieves a minimum value $\delta_\star \approx 0.0065$ at $\theta_\star \approx 0.324\pi$ and it becomes large near the edges. In MBF it was reported that the shell-summed amplitude of $\hat{F}(\boldsymbol{k})$

$$A(k) \equiv \sum_{k\le|\boldsymbol{k}|\le k+1} |\hat{F}(\boldsymbol{k})|, \tag{29}$$

a kind of discrete angle average, behaves as $C' k^{-2.16} \mathrm{e}^{-\delta_\star k}$ for large k. This is consistent with the present result. Indeed for large k, we can evaluate the shell sums (29) by integrating over $k\mathrm{d}\theta$ using (23) and steepest descent near $\theta_\star$. This changes the prefactor from $k^{-\alpha}$ to $k^{-\alpha+1-1/2} \approx k^{-2.16}$.

Finally, $C(\theta)$ is quite flat in the interval $0.1 < \theta < 0.4$.

3.3. Non-universality of the scaling exponent

Having established the angle-independence of the prefactor exponent, we now investigate its dependence on the initial condition. What happens when we change from the SOC (given by (2)) to another initial condition? Since 35-digit computations take up to one month of CPU, we generally used 15-digit

the method used in MBF was less accurate than the present one and there are thus small discrepancies in the values reported.

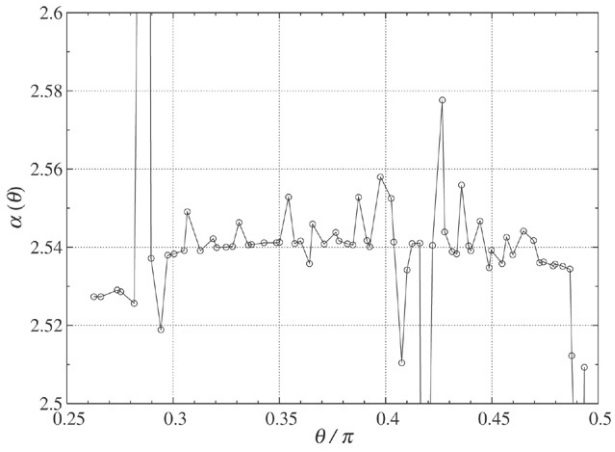

Fig. 9. Angular dependence of the prefactor exponent $\alpha(\theta)$ for the "45-degree" initial condition $\Psi_0(\boldsymbol{x}) = \cos 2x_1 + \cos(x_1 + x_2)$.

accuracy but there is one important exception (see below). At first we changed the SOC to

$$\Psi_0(\boldsymbol{x}) = \cos x_1 + \cos 3x_2, \tag{30}$$

for which the basic modes in the short-time asymptotics are (1, 0) and (0, 3) between which there is the same 90-degree angle as for the SOC. The prefactor exponent was again indistinguishably close to 8/3. For a while this led us to conjecturing the universality of the 8/3 exponent. Well ... until we tried

$$\Psi_0(\boldsymbol{x}) = \cos(x_1 + x_2) + \cos 2x_2, \tag{31}$$

whose basic modes are (1, 1) and (0, 2), forming an angle of 45 degrees. This gave us an exponent $\alpha \approx 2.54$. The same exponent was obtained with

$$\Psi_0(\boldsymbol{x}) = \cos(x_1 + x_2) + \cos px_2, \tag{32}$$

with $p = 1, 3, 4$, whose basic modes are different but also form an angle of 45 degrees. We also did some exploration of the direction dependence of α and, just as for the SOC, did not find any. As we shall see in Section 4.3, independence on the direction can be shown to hold.

All this was pointing towards non-universality of the prefactor exponent, that is dependence on the initial condition or at least on the angle between the basic modes. To ascertain the non-universality we performed a 100-digit computation for (31) with $k_{\max} = 1000$. Fig. 9 gives the epsilon-algorithm extrapolated values of the local prefactor exponent for this calculation as a function of θ.

Except near the edges the exponent stays very close to 2.54.[14] The discrepancy between 2.54 and 2.66 vastly exceeds the estimated error on the prefactor exponent, as discussed in Section 3.1. Finally, we report that for all cases discussed in this section on non-universality, the positivity of all the Fourier coefficients except one holds, just as for the SOC.

[14] The anomalously low value around $\theta/\pi = 0.42$ is caused by a large denominator in the corresponding slope (79/21) which does not permit a reliable determination of α.

3.4. Intermediate asymptotics near the edges

In this section we discuss only the SOC, but the theoretical results presented are easily generalized. We have seen that on any line of strictly positive and finite rational slope the Fourier coefficients decrease exponentially at high k (up to algebraic prefactors). This is not true for lines of vanishing and infinite slope. We can explicitly calculate from the recursion relation (12) all the coefficients having either $k_2 = 2$ or $k_1 = 1$. Indeed along such "edge lines" the recursion relations take the form of first-order linear homogeneous finite difference equations

$$\hat{F}(k_1, 2) = \frac{1}{k_1} \frac{k_1^2 - 2k_1 + 4}{k_1^2 + 2^2} \hat{F}(k_1 - 1, 2), \tag{33}$$

$$\hat{F}(1, k_2) = \frac{2}{k_2} \frac{k_2^2 - 4k_2 + 1}{1 + k_2^2} \hat{F}(1, k_2 - 2). \tag{34}$$

At large orders, essentially each coefficient on a horizontal or vertical edge line is obtained by dividing by k_1 or $k_2/2$ the adjacent lower-order coefficient. Thus they are decreasing roughly as $1/k_1!$ or $1/(k_2/2)!$. More precisely, using standard asymptotic methods for difference equations [32], it is easily shown that for integer $m \to \infty$

$$\hat{F}(m, 2) \sim \hat{F}(1, 2m) \sim m^{-5/2} \mathrm{e}^m m^{-m}, \tag{35}$$

which decreases faster than exponentially.

If we now consider a "near edge" direction with θ close to 0 or to $\pi/2$ we expect that the edge behavior will manifest itself as intermediate asymptotics making it hard to obtain clean scaling for the prefactor. We can however easily predict the θ-dependence of the decrement δ by the following argument. When θ is small, the line through the origin of slope $\tan\theta \approx \theta$ will intersect the edge $k_2 = 2$ at $k_1 \approx 2/\theta$. At this point, by (35), the logarithm of the Fourier amplitude is given to leading order by $-(2/\theta)\ln(2/\theta)$. Assuming that, on the line of slope θ, this point is within the region of exponential fall-off with decrement $\delta(\theta)$, we obtain

$$-(2/\theta)\ln(2/\theta) \approx -(2/\theta)\delta(\theta), \tag{36}$$

which gives (for $\theta \to 0$)

$$\delta(\theta) \approx \ln\left(\frac{2}{\theta}\right). \tag{37}$$

Near the other edge, we obtain by a similar argument (for $\theta \to \pi/2$)

$$\delta(\theta) \approx \frac{1}{2} \ln\left(\frac{1}{\pi - 2\theta}\right). \tag{38}$$

We turn now to numerical study of the near edge behavior of Fourier coefficients. So far we have determined such coefficients in regions having comparable extensions in the k_1 and k_2 directions. The structure of the recursion relation allows us however to determine the coefficients in rectangular domains having a very small or very large aspect ratio. We have seen that the local prefactor exponent behaves non-monotonically with the wavenumber when θ is below a critical value.[15] Consistently, we have found that for small θ's a more complex behavior is observed than for θ's close to $\pi/2$. We have thus studied the former in more detail. Because of the slow convergence to asymptotics we need wavenumbers much larger than in MBF, so we used rectangular domains of size 4000×480 near $\theta = 0$ and of size 200×4000 near $\theta = \pi/2$. Fig. 10 shows the variation with the wavenumber of the local prefactor exponent $\alpha_{\mathrm{loc}}(k)$ for various small θ's. It is seen that when θ decreases, the wavenumber at which $\alpha_{\mathrm{loc}}(k)$ achieves its minimum increases and thus the extrapolation of α becomes more difficult. The situation is much more favorable for the determination of the decrement, because it is (logarithmically) large.

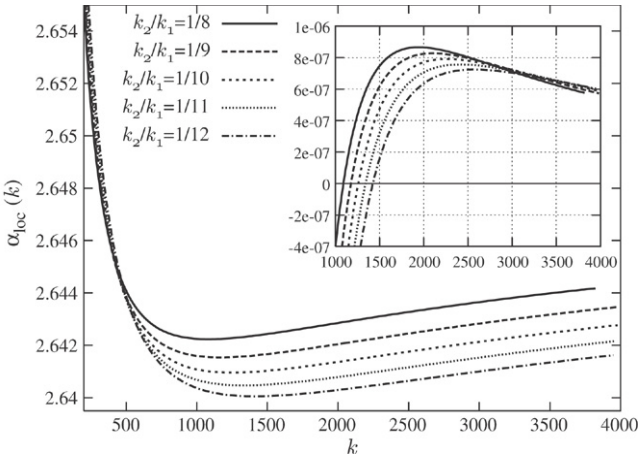

Fig. 10. Wavenumber dependence of local prefactor exponent α_{loc} for various small θ. Inset: $\mathrm{d}\alpha_{\mathrm{loc}}(k)/\mathrm{d}k$.

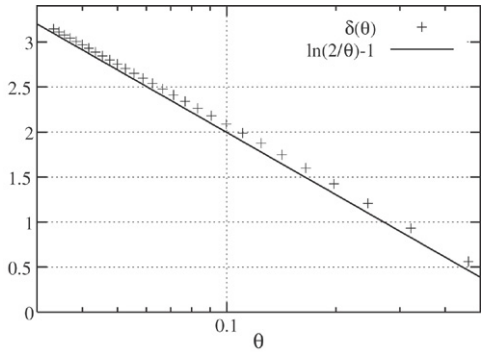

Fig. 11. Angle dependence of the decrement δ for small θ in lin–log coordinates (crosses). The continuous line is the theoretical prediction.

Fig. 11 shows the measured decrement together with a theoretical prediction $\delta(\theta) = \ln(2/\theta) - 1$ which includes a subleading correction to the leading-order prediction (37), obtained by a partially heuristic procedure. Near $\theta = \pi/2$ the decrement has also logarithmic scaling (not shown), consistent with the leading-order prediction (38) but not very clean. As to the constant $C(\theta)$, we found that it becomes large near the edges. For $\theta \to 0$ the behavior is roughly $C(\theta) \propto 1/\theta$ but

[15] This may be related to the fact that the global structure seen in Fig. 14 is far from being symmetrical in y_1 and y_2.

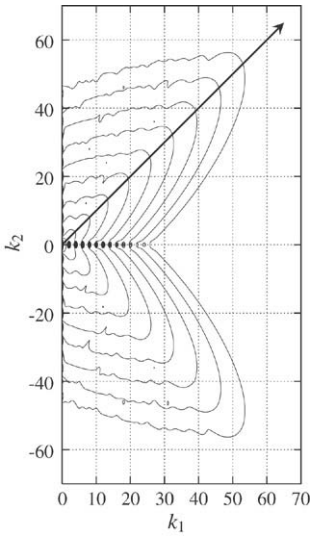

Fig. 12. Contours of the absolute value of the Fourier coefficients (logarithmic scale) of the stream function at $t = 0.8$ by full spectral simulation for the SOC.

there are substantial uncertainties because the constant C is quite sensitive to small errors made on δ and α.

3.5. Beyond short times

In MBF it was shown, for the SOC initial condition, that deviations from short-time asymptotics become important around $t = 0.1$. More precisely, deviations from the law $\delta(t) \propto \ln(1/t)$ become visible (see Fig. 2 of MBF). We now investigate numerically the issue of persistence of the $k^{-2.66}$ law for the SOC beyond the time of validity of short-time asymptotics. For this we must use a full spectral simulation with time-marching as in Refs. [4,12]. A priori there is no need to use a resolution in excess of 1024^2 since we shall see that the $k^{-2.66}$ law deteriorates significantly after $t = 1$. At that time, the decrement $\delta \approx 0.4$, which implies that the flow is extremely well resolved with 1024^2 modes. Fig. 12 shows the behavior of the absolute value[16] of the Fourier coefficients of the stream function at $t = 0.8$ in the (k_1, k_2)-plane (because of the Hermitian symmetry we are not showing negative k_1). It is seen that there is a direction of slowest decrease which has $k_2/k_1 \approx 1$. At short times the slowest decrease had $k_2/k_1 \approx 18/11$ but this direction changes in the course of time. Fig. 13 shows the usual exponential decrease with an algebraic prefactor for the Fourier amplitude in the direction of slope unity at $t = 0.8$. Beyond wavenumber 85, rounding errors take over (the calculation has 15-digit precision). The same procedure, applied at much later times, for example at $t = 1.9$, still shows some kind of exponential tail but the data are far too wiggly to permit the extraction of a reliable power-law prefactor. We have also repeated the analysis beyond short times for the flow with initial condition $\cos(x_1 + x_2) + \cos 2x_2$, where the basic modes make an angle of 45 degrees. At time $t = 1.4$ the prefactor exponent is around 2.58, quite close to the value 2.54 reported at short times.

[16] Because of the symmetry of the SOC, the Fourier coefficients are real.

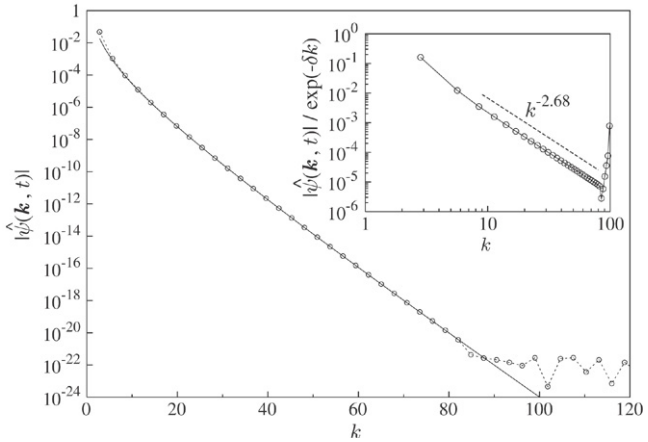

Fig. 13. Absolute value of the Fourier coefficients of the stream function at $t = 0.8$ along the rational direction $k_2/k_1 = 1$ in lin–log coordinates. A least square fit (continuous line) gives $ck^{-2.68}e^{-0.429k}$. The inset shows the same data after division by $e^{-0.429k}$ in log–log coordinates.

Let us now discuss some of the limitations involved in the search for prefactor scaling beyond the short-time asymptotics. We begin with practical limitations. With 1024^2 modes the direction of rational slope $k_2/k_1 = 1$ has about 30 points before encountering 15-digit rounding level. Other directions have typically only ten points and this makes precise determination of the decrement δ and the prefactor exponent α impossible. We thus cannot comment on any possible angular dependence of α. Calculations with higher resolution require higher precision in order to lower the rounding noise level and this in turn requires enormous computer resources by a time-marching full spectral method if we demand that temporal truncation error be at rounding level.

There is a more fundamental issue regarding the validity of the short-time asymptotic régime. For the SOC, this régime breaks down around $t = 0.1$, as far as the temporal behavior of $\delta(t)$ is concerned. Actually the short-time approximation is strongly non-uniform with respect to the wavenumber: high wavenumbers show discrepancies at much earlier times than 0.1. For example we know that, in the short-time régime, all the Fourier coefficients except one are non-negative, but as early as $t = 10^{-3}$, a 90-digit calculation by time-marching shows that Fourier coefficients start oscillating in sign beyond wavenumber forty.[17] By $t = 0.8$ such oscillations are found in the 15-digit calculation whenever $k_2/k_1 > 2$, irrespective of wavenumber. In the presence of such oscillations, the functional form we have used in the short-time asymptotics $\propto k^{-\alpha}e^{-\delta k}$ is clearly invalid. What is happening has a geometric interpretation which is more readily understood after reading the first page of Section 4. In the short-time régime the positivity of the Fourier coefficients implies that the singular manifold is in the y-plane. Note, however, that in this régime we are ignoring interactions with Fourier harmonics

[17] It matters how precisely we let $t \to 0$ and $k \to \infty$. For a fixed value of t, however small, the high-k régime discussed in most of this paper may be just an intermediate asymptotic régime. It is conceivable that the non-universality found here is confined to this particular asymptotic régime.

from quadrants other than the first one since they only contribute subdominant terms in the short-time expansion of the hydrodynamic fields. When such terms are taken into account it is likely that singularities obtained at leading order will be mostly advected by a modified velocity field which carries the singularities slightly out of the y-plane without changing their nature, as happens in the work of Tanveer and Speziale [18]. Of course, positivity of the Fourier coefficients will be lost but not necessarily their scaling properties. Observe also that the y-plane being a plane of symmetry, this picture implies that there are several pieces of the singular manifold very close to the y-plane. In Fourier space they produce a kind of interference pattern which at first has very long wavelength (in k). This wavelength becomes shorter and shorter as time advances and the singular manifold moves further away from the y-plane.[18]

4. The geometry of the pseudo-hydrodynamic flow

In two-dimensional simulations of hydrodynamics, considerable insight is usually obtained by looking at flow features in the physical space. This is much simpler in two dimensions than in three, provided that the relevant features are in the *real* $\mathbb{R}^2$ space. Here the most important features are in the *complex* $\mathbb{C}^2$ space, which is equivalent to having four real dimensions. Fortunately, as explained in Section 2, we can make use of only two real dimensions by working in the y-plane above $(z_1, z_2) = (\pi, 0)$ which extends in the (pure) imaginary directions. As already briefly mentioned in Section 4 of MBF, the positivity of all the Fourier coefficients $\hat{F}(k_1, k_2)$ (except $\hat{F}(1, 0)$) and the exponential decrease with the wavenumber imply that the solution to the (short-time asymptotic) Euler equation has a line of singularities $\mathcal{S}$ in the (y_1, y_2)-plane. Indeed, since only harmonics with non-negative k_1 and k_2 are present, we may rewrite (13) and (14) as a Taylor series in two variables

$$\psi(\mathbf{y}) - \frac{1}{2}y_1 + y_2 = \sum_{k_1=0}^{\infty}\sum_{k_2=0}^{\infty} \hat{F}(k_1, k_2)\, \zeta_1^{k_1}\, \zeta_2^{k_2}, \tag{39}$$

$$\zeta_1 \equiv \mathrm{e}^{y_1}, \quad \zeta_2 \equiv \mathrm{e}^{y_2}. \tag{40}$$

If we now hold y_2 (and thus ζ_2) fixed and sum over k_2, we obtain a Taylor series in ζ_1 such that all its coefficients (except possibly the first one) are positive. By Vivanti's theorem [33], if such a series has a finite radius of convergence (as is the case here because of the aforementioned exponential decrease), the singularity in the complex ζ_1-plane nearest to the origin is on the positive real axis at a location $y_1 = y_1^\star(y_2)$, which depends on y_2. The function $y_1^\star(y_2)$ defines an object which we here call the *singular manifold* and is the edge of the analyticity domain $y_1 < y_1^\star(y_2)$.[19] A standard theorem about multi-dimensional Taylor series states that their domain of convergence is logarithmically convex (see, e.g., Ref. [34]).

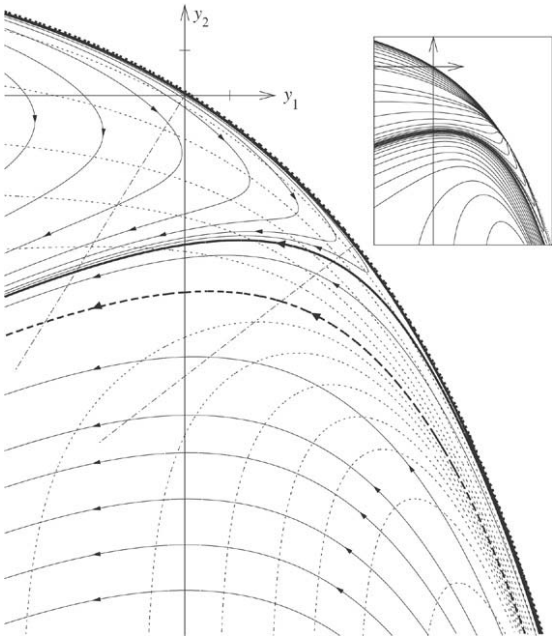

Fig. 14. Global geometry of the flow in the y-plane. Streamlines (solid lines) and iso-vorticity lines (thin-dotted lines) are shown. Thick-solid-crenated line: singular manifold; thick-solid line: U-turn separatrix ($\psi \approx 0.5$); thick-dashed line: vorticity separatrix ($\omega = 0$ and $\psi = \ln 2$). The ticks on the two axes correspond to coordinate 0.25. Inset: Contours of absolute value of the cotangent of the angle between the streamlines and the iso-vorticity lines as a measure of depletion of nonlinearity.

In our case this just means that the analyticity domain in the y-plane is convex. As shown in MBF using slightly different notation, the singular manifold can be constructed either as the envelope of the family of straight lines $y_1 \cos\theta + y_2 \sin\theta = \delta(\theta)$ (where the decrement δ has been defined in Section 3) or as the envelope of analyticity disks.

To numerically construct the pseudo-hydrodynamic solution in the y-plane from the Fourier data we use (14) for the stream function, (18) for the velocity and (20) for the vorticity. Although our Fourier data typically have 35 decimal digits, it suffices to truncate them to 16 digits to obtain the various relevant fields in y-space with a good accuracy.

4.1. Presentation of the y-plane results

We begin with global topological features and then turn to a more local and more quantitative description. Fig. 14 gives a global view of the flow in the y-plane.[20] The outer edge of the flow region, which passes very close to the origin is the singular manifold. At large distances on the upper left and the lower right, respectively, the singular manifold has logarithmic branches. Close to the singular manifold, the streamlines follow it until they make a U-turn and eventually plunge into the third quadrant ($y_1 < 0, y_2 < 0$) where they become straight with slope $1/2$ at large distances. An important feature is the U-*turn separatrix*, above which stream lines make U-turns which

[18] Somewhat similar interference patterns are obtained when the short-time asymptotics is extended to the Navier–Stokes equation (with viscosity scaling as $1/t$).

[19] More correctly, the singular manifold is a (perhaps analytic) manifold in $\mathbb{C}^2$ whose intersection with the y-plane is designated here by the same name.

[20] When magnifying this figure, ADOBE READER® 7 or higher is recommended.

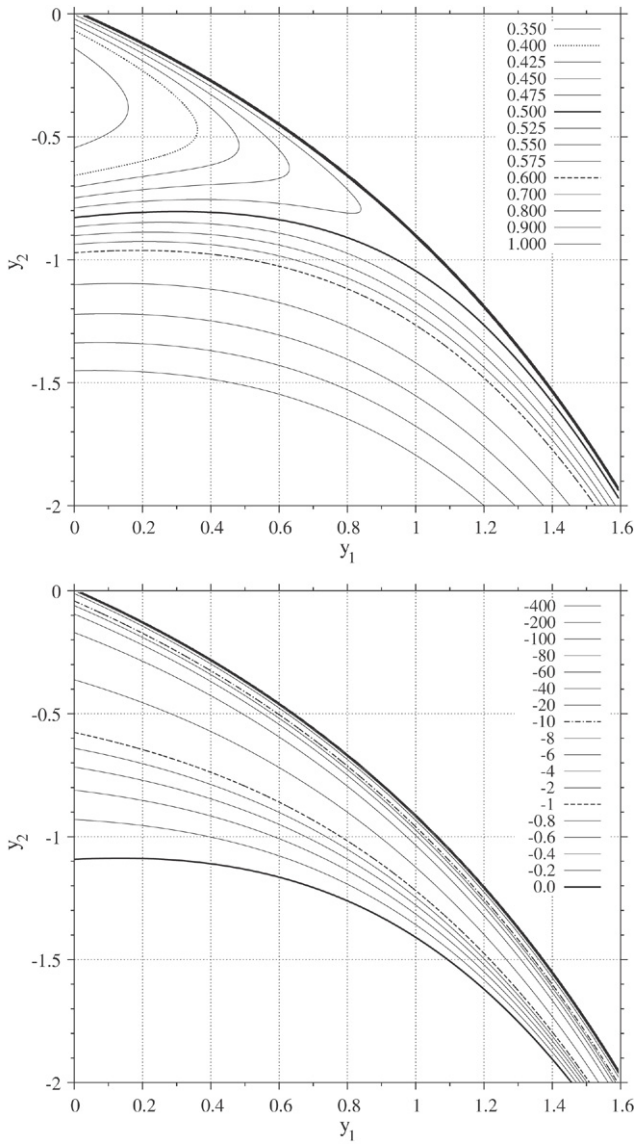

Fig. 15. Enlargements of Fig. 14 around the point $(y_1, y_2) = (0.8, -1.0)$ showing the streamlines (upper figure) and the vorticity contours (lower figure). Only negative vorticity contours are shown.

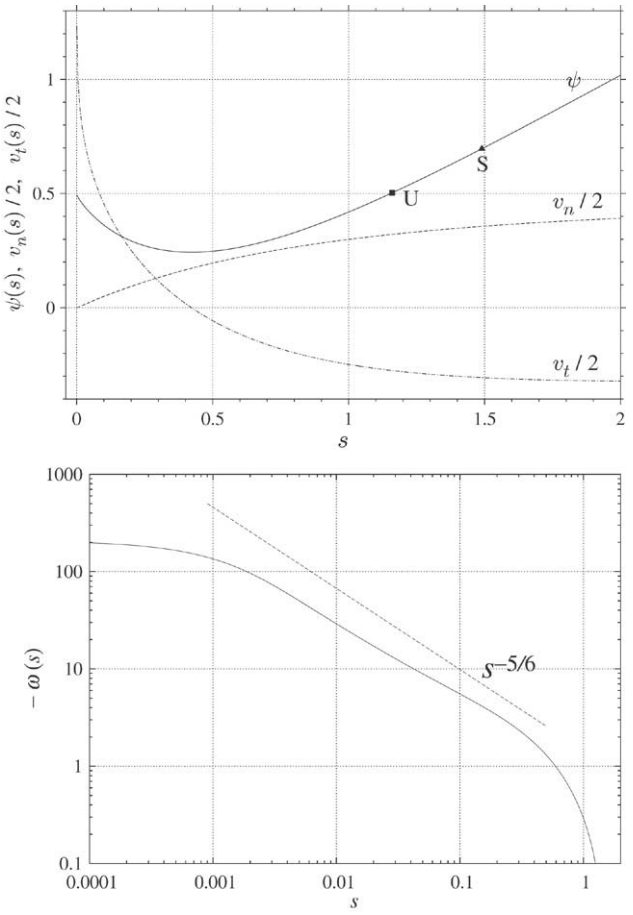

Fig. 16. Upper figure: stream function ψ, velocity components (suitably rescaled) v_n and v_t normal and parallel to the singular manifold along the line of cut normal to the singular manifold passing through the origin, shown as a dashed-dotted line on Fig. 14. U and S identify the places where the cut intersects the U-turn separatrix and the vorticity separatrix. Lower figure: negative vorticity along the same cut in log–log coordinates.

become increasingly sharp when moving to the lower right, and below which there are no U-turns. Vorticity contours starting close to the singular manifold far on the upper left get pressed increasingly close into the singular manifold when moving to the lower right. The *vorticity separatrix* divides negative vorticity (above) and positive vorticity (below). It approaches the singular manifold in the lower right but not as fast as the U-turn separatrix. In view of the Jacobian formulation of the Euler equation, the vorticity separatrix is clearly also a streamline. Hence, the strong depletion of nonlinearity evidenced by accumulation of contour lines near this separatrix on the inset of Fig. 14. The depletion is here measured by plotting the absolute value of the cotangent of the angle between $\nabla\psi$ and $\nabla\omega$.

Fig. 15 shows the stream function and the vorticity with more details in a region of particular interest. Increasingly sharp U-turns of the stream lines are seen when moving to the lower right into the narrowing channel separating the singular manifold from the U-turn separatrix. It is seen that the vorticity becomes very large and negative near the singular manifold, while the stream function remains finite with a value around $\psi = 0.5$, the same as on the U-turn separatrix. Thus, the singular manifold, which is simultaneously a limiting case of a streamline and of a vorticity contour, displays strong depletion of nonlinearity as seen on the inset of Fig. 14. We also looked at the velocity field (not shown); close to the singular manifold the velocity is parallel to this manifold and decreases in modulus when moving down and to the right. Note that, contrary to the vorticity, the velocity does not grow explosively when approaching the singular manifold; there is no numerical evidence against the plausible assumption that the velocity has a finite limit on the singular manifold which is tangent to this manifold. Similarly, the pressure (not shown) also appears to have a finite limit on the singular manifold.

For a better quantitative grasp we show in Fig. 16 a one-dimensional cut of the two-dimensional fields along the normal to the singular manifold passing through the origin, shown as a dashed-dotted line on Fig. 14. It is seen that the stream

function takes the finite value $\psi_{\text{sing}} \approx 0.5$ on the singular manifold and the same value at the U-turn separatrix and that the vorticity follows approximately a power law $-\omega \propto s^{-\beta}$ with $0.7 < \beta < 0.9$, where s is the distance to the singular manifold. The scaling is however rather poor; it gets even worse when repeating the same analysis along the other dashed line normal to the singular manifold, shown on Fig. 14. It is also seen that at the singular manifold the normal velocity vanishes linearly. We now turn to comments and theoretical explanation of most of these features.

4.2. Bridging k-space and y-space results

As we shall now see, it is quite obvious to relate the *leading-order* asymptotics (23) of the Fourier coefficients at large k and the *leading-order* behavior near the singular manifold in y-space. To explain the poor scaling observed for the vorticity in y-space, we need to take into account subleading corrections as we shall also discuss. The "Fourier–Laplace" representations (14), (18) and (20) for the (pseudo-hydrodynamic) stream function, the velocity and the vorticity, connect k- and y-space functions. Consider, for example, the vorticity; using (23) and polar coordinates $\boldsymbol{k} = k(\cos\theta,\ \sin\theta)$ we can rewrite it as

$$\omega(\boldsymbol{y}) = -\sum_{\boldsymbol{k}} C(\theta) k^{-\alpha+2} \mathrm{e}^{-kh(\theta;\boldsymbol{y})}, \tag{41}$$

$$h(\theta;\boldsymbol{y}) \equiv \delta(\theta) - y_1\cos\theta - y_2\sin\theta. \tag{42}$$

The convergence properties at high wavenumbers of this sum will depend crucially on the sign of the decrement $h(\theta;\boldsymbol{y})$. If

$$\min_{\theta} h(\theta;\boldsymbol{y}) > 0, \tag{43}$$

all the exponentials are decaying and the sum will be finite. If the minimum is negative, the sum is divergent. In the borderline case of a vanishing minimum, the algebraic prefactors will determine convergence. If $\delta(\theta)$ is a smooth function of θ, as our numerical results suggest, the minimum corresponds to a vanishing derivative with respect to θ. Hence, the borderline case is characterized by the following two equations:

$$\delta(\theta) - y_1\cos\theta - y_2\sin\theta = 0, \tag{44}$$

$$\delta'(\theta) + y_1\sin\theta - y_2\cos\theta = 0, \tag{45}$$

where $\delta'(\theta)$ is the derivative of $\delta(\theta)$. Those points $\boldsymbol{y}_\star(\theta) = (y_{\star 1},\ y_{\star 2})$ which satisfy (44) and (45) are on the singular manifold. Conversely, $\delta(\theta)$ is the distance from the origin to the tangent at the singular manifold which has the slope $\theta - \pi/2$ (see Fig. 17). It follows that the singular manifold is the envelope of such lines. In MBF this result was derived by Poincaré's pinching argument.

From (44) and (45) it is easily shown that the near-edge behavior of $\delta(\theta)$ given by (37) and (38) implies logarithmic branches for the singular manifold: $y_2 \simeq (1/2)\ln(-y_1)$ for large negative y_1 and $y_1 \simeq \ln(-y_2)$ for large negative y_2.

We observe that $s \equiv \min_\theta h(\theta;\boldsymbol{y})$ is the shortest Euclidean distance of $\boldsymbol{y}$ to the singular manifold, with a plus sign when $\boldsymbol{y}$ is below the singular manifold and a minus sign when it is above. Let us assume that $\boldsymbol{y}$ is below or on the singular manifold

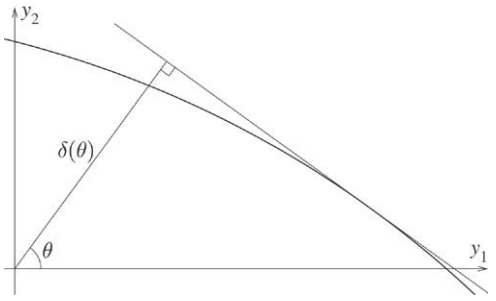

Fig. 17. Construction of the singular manifold from the logarithmic decrement $\delta(\theta)$.

and let us denote by $\theta_\star(\boldsymbol{y})$ the value of θ where the minimum is achieved. Near this minimum we can Taylor-expand the decrement

$$h(\theta;\boldsymbol{y}) = s + \frac{1}{2}h''_\star(\theta-\theta_\star)^2 + O((\theta-\theta_\star)^3), \tag{46}$$

where $h''_\star \equiv \partial^2 h(\theta_\star,\boldsymbol{y})/\partial\theta^2$. The convergence of the sum (41) depends only on the high-k behavior, where we can, to leading order, replace the sum by an integral over $k\mathrm{d}k\mathrm{d}\theta$, to obtain a "continuous approximation"

$$\omega_{\text{cont}}(\boldsymbol{y}) = -\int_0^{2\pi}\mathrm{d}\theta\int_0^\infty \mathrm{d}k\, C(\theta)k^{-\alpha+3}\,\mathrm{e}^{-kh(\theta;\boldsymbol{y})}. \tag{47}$$

When s vanishes or is small and positive, we can evaluate the angular integral in (47) by steepest descent

$$\omega_{\text{cont}}(\boldsymbol{y}_\star) \simeq -C(\theta_\star)\sqrt{\frac{2\pi}{h''_\star}}\int_0^\infty \mathrm{d}k k^{-\alpha+5/2}\,\mathrm{e}^{-ks}. \tag{48}$$

On the singular manifold, $s = 0$ and it is clear that the integral over k is ultraviolet-divergent as soon as $\alpha \geq 3/2$. All the values of the prefactor exponent α considered in this paper are at least $5/2$ and thus give an *infinite vorticity at the singular manifold*. The same analysis applied to the stream function and to the velocity gives ultraviolet-convergent integrals. For small positive s, we obtain from (48)

$$\omega_{\text{cont}}(\boldsymbol{y}_\star) \simeq -C(\theta_\star)\sqrt{\frac{2\pi}{h''_\star}}\,\Gamma(7/2-\alpha)\,s^{-\beta}, \tag{49}$$

$$\beta = \frac{7}{2} - \alpha, \tag{50}$$

where $\Gamma(\cdot)$ denotes the Gamma function.

For SOC initial conditions, $\alpha \approx 8/3$, and thus the vorticity diverges to leading order with a $s^{-5/6}$ law, when approaching the singular manifold. The subleading corrections causing the poor scaling seen in Section 4.1 are of various sorts. First, there are subleading corrections to (23) whose simplest manifestation is the discrepancy between the local scaling exponent $\alpha_{\text{loc}}(k)$ and its extrapolated value α_∞, as discussed in Section 3.1. As already stated, we do not know the functional form of such corrections. Second, there are subleading corrections coming from having approximated the Fourier–Laplace sums by integrals. It is easily shown that they contribute $O(s^0)$ to the

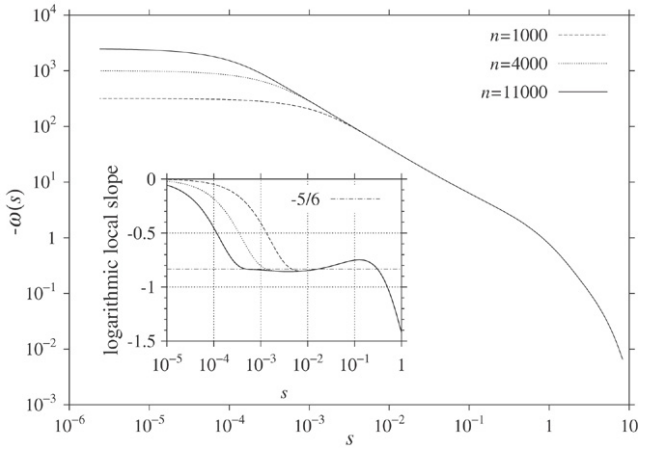

Fig. 18. Same as lower part of Fig. 16 but for the synthetic data with various values of the maximum wavenumber n. Inset: corresponding logarithmic local slopes. The predicted scaling exponent is $-5/6$.

vorticity in y-space. Third, there are the subleading corrections to the continuous approximation (47), which may be shown to be $O(s^{-1/3})$. A simple way to determine how much the scaling is degraded by the second and third type of corrections is to use *synthetic data* for which the Fourier coefficients are given exactly by (23). It is then easy to change the resolution $n \times n$ and to find out how large n should be for clean leading-order scaling to emerge. We performed such a calculation with C and α constant and the values of $\delta(\theta)$ taken from the actual Euler SOC data. From the synthetic data, using (20) we then calculate a synthetic vorticity $\omega_{\text{synth}}(\boldsymbol{y})$ just as in Section 4.1. Fig. 18 shows $-\omega_{\text{synth}}(\boldsymbol{y})$ in log–log coordinates for three values of n. The lowest one, $n = 1000$, is comparable to what is used in the actual Euler calculation: the scaling is very poor. Only when we increase the resolution more than tenfold to $n = 11{,}000$ do we begin to see a clean $s^{-5/6}$ scaling.

4.3. Theory of y-plane pseudo-hydrodynamics

The starting point for theory in the y-plane is of course the pseudo-hydrodynamic vorticity equation and its boundary conditions far into the third quadrant, derived in Section 2 and repeated here for convenience:

$$\boldsymbol{v} \cdot \nabla\omega + \omega = 0, \tag{51}$$

$$\boldsymbol{v} \simeq \left(-1,\ -\frac{1}{2}\right), \quad \omega \simeq \frac{1}{2}\mathrm{e}^{y_1} - 2\mathrm{e}^{2y_2}, \quad y_1,\ y_2 \to -\infty. \tag{52}$$

Alternatively we can rewrite (51) as $J(\psi, \omega) = \omega$ or as $J(\psi, \ln|\omega|) = 1$. Thus the map from $(y_1,\ y_2)$ to $(\psi,\ \ln|\omega|)$ is area preserving. The vorticity separatrix was defined by $\omega = 0$; so that the Jacobian of the stream function and of the vorticity is zero along this line. Hence it is also a streamline.[21] It is easily shown that the value of the streamfunction on this line is $\ln 2$. Indeed, as we follow the vorticity separatrix far into the third quadrant, we obtain from (52) that $y_1 \simeq 2y_2 + 2\ln 2$. Since $\psi = (1/2)y_1 - y_2$ (up to exponentially small terms), we obtain the result claimed. We have also checked numerically that the value of the stream function on the vorticity separatrix is $\ln 2$ to at least three decimal places.

Depletion of nonlinearity near the singular manifold prevents us from using the dynamical equation (51) to derive the scaling exponent of the singularities by, for example, balancing to leading order the two terms in (51). Nevertheless, such balancing gives some useful information, such as the vanishing of the normal component $v_n(s)$ of the velocity near the singular manifold (for $s \to 0$) and the independence on position of the exponent β characterizing the divergence of the vorticity. Since β and the prefactor exponent α are related by $\alpha + \beta = 7/2$, this will establish the independence of α on θ, which was rather strongly supported by the numerical results reported in Section 3. We now derive these results. In what follows, points $\boldsymbol{y}_\star$ on the singular manifold are parameterized by the angle θ between the y_1-axis and the outgoing normal.

To show the vanishing of $v_n(s)$ for $s \to 0$, it is convenient to use as *local coordinates* near the singular manifold the angle θ and the distance s. We denote by $v_n(s,\theta)$ and $v_t(s,\theta)$ the components of the velocity along the inward normal and along the tangent in the direction of increasing θ. For small s, to leading order, (51) becomes

$$\left[v_n(s,\theta)\partial_s + v_t(s,\theta)\frac{1}{R(\theta)}\partial_\theta\right]\omega(s,\theta) \simeq -\omega(s,\theta), \tag{53}$$

where $R(\theta)$ is the radius of curvature of the singular manifold (the arclength is given by $R(\theta)\mathrm{d}\theta$). We now assume that $\omega \propto s^{-\beta}$ (with $\beta > 0$). If $v_n(0,\theta)$ did not vanish, the first term on the l.h.s. of (53) would be proportional to $s^{-\beta-1}$, which for small s could not be balanced by any of the other terms of the equation. The argument actually implies the stronger result that the normal velocity v_n cannot vanish more slowly than s^1. The technique of Section 4.2 on bridging k-space and y-space results can be used to show that $\partial v_n/\partial s$ remains finite at the singular manifold, although it has the same dimension as the vorticity which becomes infinite.[22] Thus v_n actually vanishes linearly with s.

For the independence of β on θ, we integrate (51) along a typical streamline passing near the singular manifold between two points M_0 (far from the singular manifold) and M_1 (within a small distance s_1), so that there is a U-turn in between which is assumed not to be close to either M_0 or M_1 (see Fig. 19). We obtain

$$\frac{\omega(M_1)}{\omega(M_0)} = \exp\left\{\int_{M_0}^{M_1}\frac{\mathrm{d}\ell}{|\boldsymbol{v}(\ell)|}\right\}. \tag{54}$$

The streamline is here parameterized by the arclength ℓ measured from an arbitrary reference point and growing when moving into the upper far left, opposite to the direction of

[21] By changing ω into $1/\omega$ in (51), we can show similarly that the singular manifold, at which $1/\omega = 0$, is also a streamline.

[22] In the proof one uses the vanishing of the normal component of the velocity at the singular manifold, a consequence of the singular manifold being a streamline.

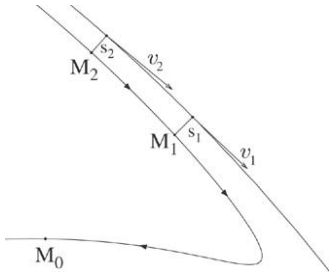

Fig. 19. A typical streamline passing near the singular manifold and performing a U-turn. Although this figure uses the actual data rather then being a sketch, the distance between the streamline and the singular manifold has been somewhat increased for legibility.

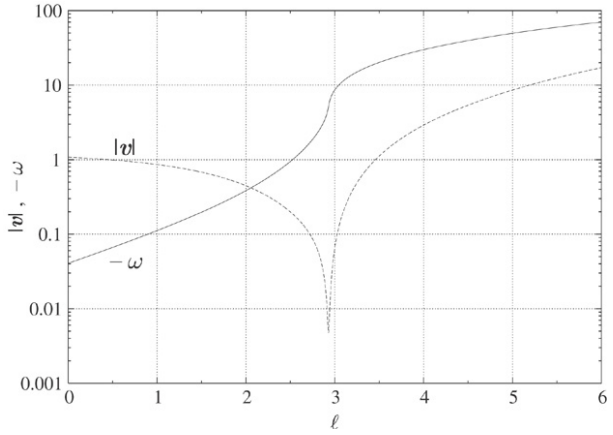

Fig. 20. Modulus of the velocity and vorticity (changed sign) versus arclength ℓ along the streamline shown in Fig. 19 which has $\psi \approx 0.47$. The point M_0 is taken near $\ell = 2.5$; the U-turn, M_1 and M_2 are near $\ell = 3$, $\ell = 3.2$, $\ell = 3.5$, respectively.

the velocity. When moving from M_0 to M_1 the smallest velocities and thus the leading-order contribution to the integral $\int_{M_0}^{M_1} \mathrm{d}\ell/|\boldsymbol{v}(\ell)|$ are expected to come from the immediate neighborhood of the U-turn. We have checked this conjecture numerically by calculating the vorticity and the modulus of the velocity along a streamline chosen to have a rather sharp but well-resolved U turn (see Fig. 20).

We assume now that the vorticity near the singular manifold is given to leading order by $\omega = c(\theta)s^{-\beta(\theta)}$, where we temporarily leave the possibility that the exponent β depends on the parameter θ associated to the nearest point on the singular manifold. We take a second point M_2 on the same streamline but further away from the U-turn. We then have (to leading order)

$$\omega(M_1) \simeq c(\theta_1)s_1^{-\beta(\theta_1)}, \tag{55}$$

$$\omega(M_2) \simeq c(\theta_2)s_2^{-\beta(\theta_2)}, \tag{56}$$

where $(s_1,\ \theta_1)$ and $(s_2,\ \theta_2)$ are the local coordinates for M_1 and M_2. From (54), applied successively to M_1 and M_2, we find that

$$\frac{\omega(M_2)}{\omega(M_1)} \simeq \exp\left\{\int_{M_1}^{M_2} \frac{\mathrm{d}\ell}{|\boldsymbol{v}(\ell)|}\right\}. \tag{57}$$

Between M_1 and M_2 the streamline is close to the singular manifold and the velocity is dominated by its tangential component; hence we can replace the r.h.s. of (57) by an integral along the singular manifold and obtain to leading order

$$\frac{\omega(M_2)}{\omega(M_1)} \simeq K_{12} \equiv \exp\left\{\int_{\theta_1}^{\theta_2} \mathrm{d}\theta\, \frac{R(\theta)}{v_t(\theta)}\right\}, \tag{58}$$

which depends neither on s_1 nor on s_2. We now observe that the solenoidal character of the velocity implies (again to leading order)

$$s_1 v_t(\theta_1) \simeq s_2 v_t(\theta_2). \tag{59}$$

It follows from (58) and (59) that

$$\omega(M_2) \simeq c_2\left[\frac{s_1 v_1}{v_2}\right]^{-\beta(\theta_2)} \simeq K_{12}\, c_1 s_1^{-\beta(\theta_1)}. \tag{60}$$

Comparison of the middle and the rightmost members gives

$$\beta(\theta_1) = \beta(\theta_2), \quad c_2 = K_{12}\, c_1 \left[\frac{v_1}{v_2}\right]^{\beta}. \tag{61}$$

This establishes the independence of the vorticity scaling exponent on θ.

5. A passive scalar model

As shown in Ref. [35], simple advection of a passive scalar by a prescribed velocity field with just a few Fourier harmonics can easily lead to singularities because fluid particles may come from or go to (complex) infinity in a finite time. In the present context of short-time asymptotics, the equivalent of a passive scalar model is to treat the (pseudo-hydrodynamic) vorticity ω in (21) as a passive scalar advected by a prescribed velocity. The simplest prescribed velocity we can take is

$$\boldsymbol{v}_{\mathrm{P}}(\boldsymbol{y}) = \left(-1,\ -\frac{1}{2}\right) + \left(\mathrm{e}^{2y_2},\ \frac{1}{2}\mathrm{e}^{y_1}\right), \tag{62}$$

obtained from the stream function

$$\psi_{\mathrm{P}} \equiv \frac{1}{2}y_1 - y_2 - \frac{1}{2}\mathrm{e}^{y_1} + \frac{1}{2}\mathrm{e}^{2y_2}. \tag{63}$$

This velocity field includes the drift $(-1,\ -1/2)$ resulting from the shifts of the original coordinates by terms proportional to $\ln t$ and the contributions from the basic modes. For our passive scalar model we use the vorticity equation (21) with the inclusion of an inhomogeneous term whose precise form does not matter (as long as it does not have itself any singularity): the singularities of the passive vorticity stem solely from advection. Specifically, the passive scalar model is defined by

$$\boldsymbol{v}_{\mathrm{P}} \cdot \nabla\omega + \omega = \frac{3}{2}\mathrm{e}^{y_1+2y_2}, \tag{64}$$

where the r.h.s. is taken to be the interaction term of the two basic modes. It is easy to write down Fourier-space recursion relations for this model and to show that all the Fourier coefficients are positive. Numerical solution of the recursion relations gives the usual type of scaling with a very clean

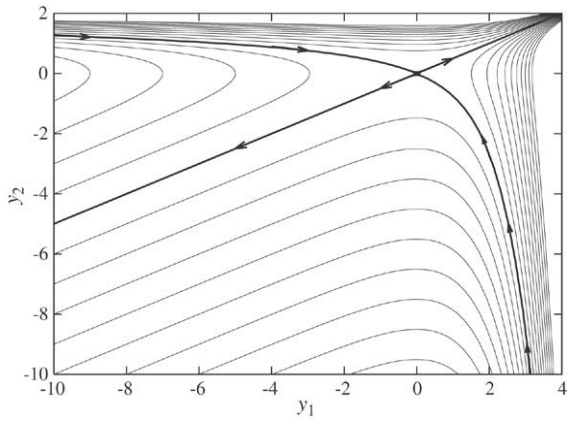

Fig. 21. Streamlines in the y plane for the passive scalar model given by (63), which has a hyperbolic stagnation point at the origin. Thick line with arrows pointing to the origin: stable manifold of the associated dynamical system (65) which is also the singular manifold for the vorticity. Thick line with arrows pointing away from the origin: unstable manifold.

prefactor exponent $\alpha = 5/2$.[23] In the y-space this implies a blow-up of the vorticity $\omega \propto s^{-1}$ as function of the distance s to the singular manifold.

Actually all these results can be derived in a rather straightforward manner by working in the y-space, as we now explain. Eq. (64) can be integrated along the characteristics. For this we consider the conservative dynamical system of fluid particle trajectories in the velocity field $\boldsymbol{v}_{\mathrm{P}}$:

$$\frac{\mathrm{d}}{\mathrm{d}\tau}\boldsymbol{y} = \boldsymbol{v}_{\mathrm{P}}(\boldsymbol{y}). \tag{65}$$

The integral lines are the lines $\psi_{\mathrm{P}} = \text{const.}$, which are shown in Fig. 21. At the origin there is a hyperbolic stagnation point near which we have $\psi_{\mathrm{P}} = -(1/4)y_1^2 + y_2^2 + O(|\boldsymbol{y}|^3)$. The associated unstable manifold is simply $y_1 = 2y_2$, while the stable manifold is the other solution to $\psi_{\mathrm{P}} = 0$.

This hyperbolic stagnation point at the origin completely determines the scaling of the vorticity. Indeed, in Section 4.3 we derived from the vorticity equation (21) an expression (54) which shows that large vorticities stem from low-velocity regions. This derivation, which did not make use of the fact that the vorticity is the curl of the velocity, remains valid for the passive scalar model (except for minor changes due to the presence of an inhomogeneous term). In the fully nonlinear case, the low velocities were due to the increasingly sharp U-turns described in Section 4.1. In the present much simpler case, they are just due to the passage near the hyperbolic stagnation point. As we follow a streamline upstream (i.e. to increasing arclengths ℓ in the notation of Section 4.3) we come closer and closer to the stable manifold. The latter thus plays the role of the singular manifold. By the same argument as used in Section 4.3 the scaling of the vorticity near the stable/singular manifold is the same everywhere. It suffices to determine it locally near the stagnation point. One way is to parameterize the streamline by the distance s to the stable manifold (more precisely to its tangent at the origin, since we are doing a local analysis). By (54), the growth of the vorticity is controlled by

$$\exp\left\{\int^{\ell} \frac{\mathrm{d}\ell'}{|\boldsymbol{v}(\ell')|}\right\} = \exp\left\{\int^{s} \frac{\mathrm{d}s'}{v_n(s')}\right\}, \tag{66}$$

where $v_n(s)$ is the velocity component along the (inward) normal $\boldsymbol{n} = (-1/\sqrt{5}, -2/\sqrt{5})$ to the stable manifold at the origin. Near a hyperbolic stagnation point we have $v_n(s) = \lambda s + O(s^2)$, where λ is the positive eigenvalue of the velocity gradient $\partial_i v_j$ at the stagnation point. Here, it is elementary to show that $\lambda = 1$. Using this in (66) we find that the vorticity $\omega \propto s^{-1}$, as claimed. This argument is easily adapted to the passive scalar models for other two-mode initial conditions, such as those discussed in Section 3.3. The same s^{-1} behavior is always obtained, which is thus universal, contrary to what happens in the full nonlinear case.

Although the passive scalar model does not predict the exact and non-universal character of the vorticity blow-up for the full nonlinear problem, the singular manifold is given quite accurately by the passive scalar model. In particular it is immediately checked that both have the same logarithmic branches (at least to leading order). Furthermore, in the passive scalar model the stable/singular manifold goes exactly through the origin while in the full nonlinear problem it passes within a distance $\delta \approx 0.0065$, as shown in MBF. It may be that such agreements are due to the presence of very strong depletion of nonlinearity in the full problem, thereby making a simple linear advection model quite relevant.

Actually, the passive scalar model can be systematically improved by enriching the prescribed velocity field through addition of higher-order modes. A simple way to do this is to take all the Fourier modes such that $k_1 + k_2/2 \leq n + 1$. For SOC, we have studied these "enriched" passive scalar models for various values of n. They all possess a hyperbolic stagnation point. The associated positive eigenvalue λ_n becomes larger than unity when $n \geq 1$. The first few values for the corresponding prefactor exponent $\alpha_n = 7/2 - 1/\lambda_n$ are: $\alpha_0 = 2.5$, $\alpha_1 \approx 2.594$, $\alpha_2 \approx 2.613$. For larger values of n, the growth is very slow; for example $\alpha_{20} \approx 2.618$. We also observed that, as n grows, the stagnation point moves to the right and down and the angle between its stable and unstable manifolds decreases. It is likely that, for $n \to \infty$, the stagnation point is pushed to infinity in such a way that its stable and unstable manifold tend to the singular manifold and to the U-turn separatrix for the nonlinear problem, while $\alpha_n \to \alpha$, but the convergence may be slow.

6. Conclusion

The present paper, like Refs. [4] and MBF, is mainly concerned with the short-time asymptotics of the 2D Euler equation in situations where complex-space singularities are born at infinity at time $t = 0+$. Let us first summarize the main findings of this work, which uses a mixture of ultra-high precision computations (with up to 100-digit accuracy) and of theory. Our work is specifically concerned with initial

[23] With the already cited asymptotic interpolation method [31] the exponent α is found to differ from 5/2 by less than 10^{-11}.

conditions in the form of a trigonometric polynomial; it is shown in the Appendix that this problem can generically be reduced to one with only two modes. A very detailed description of the complex singularities is given. For all cases studied, the Fourier coefficients except one are found to be non-negative (this was already reported for SOC in MBF). In any direction of rational slope $\tan\theta$ not too close to the edges of the Fourier domain, the coefficients of the stream function converge very quickly with increasing wavenumbers k to the form $C(\theta)k^{-\alpha}\mathrm{e}^{-k\delta(\theta)}$. The prefactor exponent α, determined with better than one per cent accuracy, is independent of θ but is not universal: when the initial modes are orthogonal, it is indistinguishable from $8/3 \approx 2.66$, whereas with a 45 degree angle between the initial modes it takes the value 2.54. We cannot rule out that α depends also on the moduli of the initial modes but we have no evidence that it does.

It is shown that the singularity problem can be reformulated as an ordinary steady-state (pseudo)hydrodynamic problem in a suitable y-plane corresponding to pure imaginary coordinates. The complex singularities are in this y-plane on a smooth (possibly analytic) curve extending to infinity with logarithmic branches. The vorticity diverges as $s^{-\beta}$, where s is the distance to the singular manifold and $\alpha + \beta = 7/2$. We give a full description of the geometry of streamlines and vorticity contours in the y-plane (Fig. 14). Increasingly sharp U-turns of the streamlines near the lower logarithmic branch of the singular manifold give rise to the vorticity scaling. Very strong depletion of nonlinearity near the singular manifold prevents application of dominant balance to determine the scaling exponent of singularities and is likely to be the reason for the very unusual non-universality of the singularities. Finally it is shown that the scaling behavior of the prefactor persists in time significantly beyond the validity of the short-time asymptotics, at least as intermediate asymptotics. However, we do not know if the non-universality of the singularities found in the short-time régime carries over to the full Euler equation.

The main theoretical shortcomings of this work are our inability so far to prove the positivity of Fourier coefficients and to derive the prefactor exponent α (or the vorticity divergence exponent β) from the initial conditions (we also failed to identify the nature of subleading corrections to (23)). We have nevertheless gained some qualitative understanding with the passive scalar model of Section 5 that ignores the back reaction of the vorticity on the velocity but which sheds interesting light on the mechanism for producing singularities. In this toy model, scaling is controlled by a stagnation point of the velocity field, whereas in the full nonlinear problem the stagnation point is rejected to infinity.

We have described our findings in some detail, hoping that colleagues will be able to help us with the missing theory.

In principle the methods used for the 2D short-time Euler problem can be extended to various other short-time problems. One instance is the short-time régime for the 2D ideal incompressible MHD equations. A preliminary study for this case indicates that the positivity result does not survive: Fourier amplitudes display oscillations revealing a richer geometry of the singular manifold which can no more be captured in terms of just the imaginary coordinates $\boldsymbol{y}$. In mathematical terms, one has to study the amoeba and coamoeba of the singular manifold.[24] Oscillations can be handled by techniques similar to those discussed here, as has already been done in Ref. [19].

Another natural extension of our study is to the 3D Euler equations which also have a short-time régime. This is rather straightforward. A direct extension of the algorithm used in two dimensions requires CPU resources (time complexity) proportional to $k_{\max}^6$ instead of $k_{\max}^4$. This becomes prohibitively large when $k_{\max}$ exceeds a few hundred. In principle, the time complexity can be reduced to $k_{\max}^3$ (with logarithmic corrections) by using FFT's and the recent technique of "relaxed multiplications" [37]. However, in the calculations reported in MBF and the present paper the magnitude of Fourier coefficients can vary by several hundred orders of magnitude; this requires special precautions when applying FFT's unless one is prepared to use several hundred digits.

We remind the reader that our long term goal is to find out about blow-up in three dimensions (3D). We hope this will not take another 250 years. Progress may however be painfully slow if, as we expect, numerical experimentation is to play an important part. Indeed, the amazingly fast growth of computer power observed over the last 50 years becomes much less spectacular when translated in terms of resolution achievable in 3D simulations.[25] As more powerful computers become available for investigation of 3D blow-up, it would not be advisable to use the new resources exclusively for increasing the spatial resolution. Experience on the advantage of ultra-high precision for singularity studies from the work of Krasny [21], Shelley [20], Caflisch [19] and also from our own work suggest that it is not safe to use less than 30–35 digits. Using flows with symmetries such as the Taylor–Green [13,14] or the Kida–Pelz [15–17] flow to boost the resolution introduces a possible element of non-genericity, but we can always use such flows to sharpen our tools and then, as computers become more powerful, turn to flows without symmetry.

Have the results reported in MBF and the present paper brought us closer to this Holy Grail of 3D blow-up? In a direct way, we cannot infer anything regarding 3D real blow-up from a 2D study of complex singularities at short times. We have however learned that in this rather restricted framework, singularities are located on very smooth objects (possibly analytic manifolds); because the fastest spatial variation is then in the direction perpendicular to the singular manifold, the singularities have strongly depleted nonlinearity in a suitable frame. We have already good evidence that in 2D this smoothness property is not limited to the short-time régime [4]. In 3D such a

[24] In d-dimensional algebraic geometry one deals with an algebraic manifold in complex coordinates $\zeta_1, \dots \zeta_d$ and the amoeba is defined as the image of the manifold under the map $\zeta_1 \mapsto y_1 \equiv \ln|\zeta_1|, \dots, \zeta_d \mapsto y_d \equiv \ln|\zeta_d|$. The coamoeba is similarly defined in terms of the argument functions of the ζ's. The complex exponentials $\mathrm{e}^{-\mathrm{i}z_1}, \dots, \mathrm{e}^{-\mathrm{i}z_d}$, play here the role of the ζ_i's. The name amoeba has been proposed by Gelfand et al. [36] because amoebae sometimes have pseudopods resembling those of microscopic protozoa. Coamoebae have been introduced by Tsikh and Passare (private communication).

[25] At the moment the highest resolution accessible in 15-digit precision for three-dimensional flow without any special symmetries is 2048^3 [38,39].

property would be both a curse, since dominant balance cannot be used, and perhaps a blessing, since it might well slow down (indefinitely?) the approach of singularities to the real domain.

Acknowledgments

We are grateful to M. Blank, H. Frisch, J. van der Hoeven, D. Mitra, A. Pumir, A. Sobolevskiĭ, A.K. Tsikh, P. Zimmermann and an anonymous referee for useful discussions and comments. Part of this work was done while the authors participated in "Frontiers of Non Linear Physics" (Nizhny Novgorod, Russia, July 5–12, 2004) and in "Singularities, coherent structures and their role in intermittent turbulence" (Warwick, UK, September 9–17, 2005). TM and JB were supported by the Grant-in-Aid for the 21st Century COE "Center for Diversity and Universality in Physics" from the Japanese Ministry of Education. TM was supported by the Japanese Ministry of Education Grant-in-Aid for Young Scientists [(B), 15740237, 2003] and by the French Ministry of Education. UF was supported by the Grant-in-Aid for the 21st Century COE "Center of Excellence for Research and Education on Complex Functional Mechanical Systems" from the Japanese Ministry of Education. WP had partial support from the European network EU RTN no. HPRN-CT-2002-00282 'Hyké. JB, UF and WP had partial support from the Fédération de Recherche Wolfgang Doeblin (FR 2800 CNRS). Part of the computational resources were provided by the Yukawa Institute for Theoretical Physics (Kyoto) and by the Mésocentre SIGAMM (Nice).

Appendix. Reduction of multimode initial conditions

Here we shall show that the short-time asymptotics of two-dimensional Euler flows with generic initial conditions of trigonometric polynomial type can be reduced to the study of two-mode initial conditions. In Section 2 we have seen that with two initial modes $\mathfrak{p}$ and $\mathfrak{q}$ the behavior of the stream function $\Psi(z,t)$ for large imaginary arguments $|y_1|$, $|y_2|$ can be described by the *similarity ansatz* (6) and (7). It relies on the fact that when $\boldsymbol{y}$ is such that $\mathfrak{p}_2/\mathfrak{p}_1 \le y_2/y_1 \le \mathfrak{q}_2/\mathfrak{q}_1$ the leading-order factors accompanying each factor t in the time–Taylor expansion (4) are either $\mathrm{e}^{-\mathrm{i}\mathfrak{p}\cdot z}$ or $\mathrm{e}^{-\mathrm{i}\mathfrak{q}\cdot z}$. In the limit $|\boldsymbol{y}| \to \infty$, $t \to 0$ we can make such terms finite by shifting simultaneously $\mathfrak{p}\cdot\boldsymbol{y}$ and $\mathfrak{q}\cdot\boldsymbol{y}$ by $\ln t$.

The similarity ansatz as explained above is however not applicable to the case of more than two initial modes. Instead, we have to reduce the multimode initial condition to various two-mode problems which can be handled in the usual way. Let us illustrate this by looking at a simple three-mode initial condition

$$\Psi_0(\boldsymbol{x}) = h_1\mathrm{e}^{\mathrm{i}\mathfrak{p}\cdot\boldsymbol{x}} + h_2\mathrm{e}^{\mathrm{i}\mathfrak{q}\cdot\boldsymbol{x}} + +h_3\mathrm{e}^{\mathrm{i}\mathfrak{r}\cdot\boldsymbol{x}} + \text{c.c.}, \tag{A.1}$$

in which the vectors $\mathfrak{p}$, $\mathfrak{q}$ and $\mathfrak{r}$ are listed in angular counterclockwise order. As in Section 2, to avoid pathologies, we assume that the vectors $\mathfrak{p}$, $\mathfrak{q}$, $\mathfrak{r}$ are not parallel and not of the same length. In the Taylor expansion (4) each factor t will now be accompanied by a factor $\mathrm{e}^{-\mathrm{i}\mathfrak{p}\cdot z}$, $\mathrm{e}^{-\mathrm{i}\mathfrak{q}\cdot z}$ or $\mathrm{e}^{-\mathrm{i}\mathfrak{r}\cdot z}$. Note that, in the limit $|\boldsymbol{y}| \to \infty$, $t \to 0$, we cannot simultaneously make the terms $t\mathrm{e}^{\mathfrak{p}\cdot\boldsymbol{y}}$, $t\mathrm{e}^{\mathfrak{q}\cdot\boldsymbol{y}}$ and $t\mathrm{e}^{\mathfrak{r}\cdot\boldsymbol{y}}$ remain finite. Indeed, we cannot translate $\boldsymbol{y}$ in such a way that all three scalar products $\mathfrak{p}\cdot\boldsymbol{y}$, $\mathfrak{q}\cdot\boldsymbol{y}$ and $\mathfrak{r}\cdot\boldsymbol{y}$ are shifted by $\ln t$. If $\mathfrak{p}_2/\mathfrak{p}_1 \le y_2/y_1 \le \mathfrak{q}_2/\mathfrak{q}_1$ the factors $t\mathrm{e}^{\mathfrak{p}\cdot\boldsymbol{y}}$ and $t\mathrm{e}^{\mathfrak{q}\cdot\boldsymbol{y}}$ will dominate, while if $\mathfrak{q}_2/\mathfrak{q}_1 \le y_2/y_1 \le \mathfrak{r}_2/\mathfrak{r}_1$ the factors $t\mathrm{e}^{\mathfrak{q}\cdot\boldsymbol{y}}$ and $t\mathrm{e}^{\mathfrak{r}\cdot\boldsymbol{y}}$ will dominate. In each case the three-mode initial condition (A.1) is reduced to a two-mode problem involving either $\mathfrak{p}$ and $\mathfrak{q}$ or $\mathfrak{q}$ and $\mathfrak{r}$.

Let us now turn to the general multimode case with an initial stream function of the form

$$\Psi_0(z_1,z_2) = \sum_{(k_1,k_2)\in\operatorname{supp}\hat{F}^{(0)}} \hat{F}^{(0)}(k_1,k_2)\mathrm{e}^{-\mathrm{i}k_1z_1}\mathrm{e}^{-\mathrm{i}k_2z_2}. \tag{A.2}$$

Here, we assume Hermitian symmetry[26] $\hat{F}^{(0)*}(k_1,k_2) = \hat{F}^{(0)}(-k_1,-k_2)$ and we take the sum over all wavevectors for which the Fourier coefficients $\hat{F}^{(0)}(k_1,k_2)$ do not vanish, called the *support* of $\hat{F}^{(0)}$ and denoted $\operatorname{supp}\hat{F}^{(0)}$. The fact that $\operatorname{supp}\hat{F}^{(0)}$ is a finite set plays a crucial part in our analysis. Let us suppose for simplicity that all initial modes have different lengths, that is $|(k_1',k_2')| \ne |(k_1'',k_2'')|$ for all pairs (k_1',k_2') and $(k_1'',k_2'') \in \operatorname{supp}\hat{F}^{(0)}$.

As we have seen before, it is necessary to distinguish between different directions in the $\boldsymbol{y}$-space when taking the limits $|\boldsymbol{y}| \to \infty$, $t \to 0$. Therefore we let $|y_1|, |y_2| \to \infty$ while keeping the ratio y_2/y_1 fixed. By Hermitian symmetry, it is enough to consider only the case $y_1 \to +\infty$. Assuming as in Section 2 that

$$\Psi(z,t) = \sum_{n=0}^{\infty} \Psi_n(z)\, t^n, \tag{A.3}$$

and denoting by $\hat{F}^{(n)}(\boldsymbol{k})$ the Fourier coefficients of Ψ_n we obtain easily from the Euler equation the following recursion relations for the Fourier coefficients of the $(n+1)$th "generation":

$$\hat{F}^{(n+1)}(k_1,k_2) = -\frac{1}{n+1}\frac{1}{|k|^2} \times \sum_{m+p=n}\sum_{\boldsymbol{k}'+\boldsymbol{k}''=\boldsymbol{k}} (\boldsymbol{k}'\wedge\boldsymbol{k}'')|\boldsymbol{k}''|^2\hat{F}^{(m)}(k_1',k_2')\hat{F}^{(p)}(k_1'',k_2''), \tag{A.4}$$

which allows us to compute $\hat{F}^{(n+1)}(\boldsymbol{k})$ in terms of the previous generations $\hat{F}^{(m)}(\boldsymbol{k})$ and $\hat{F}^{(p)}(\boldsymbol{k})$ with $m, p \ge 0$ and $m+p=n$. From (A.4) it follows immediately that $\hat{F}^{(n)}$ has finitely many non-vanishing modes.

We now identify the modes in the nth generation which give the leading-order contributions to $\Psi_n(z)$ for a fixed ratio y_2/y_1. For this we use the notion of *Newton polytope* of $\operatorname{supp}\hat{F}^{(0)}$. It is defined as the convex hull (in the usual sense) of the set $\operatorname{supp}\hat{F}^{(0)}$, as for example represented (taking into account the Hermitian symmetry) on Fig. 22 for a typical initial condition. We shall call *relevant* those initial modes lying on the boundary of the Newton polytope of $\operatorname{supp}\hat{F}^{(0)}$ (black circles indicated by arrows on Fig. 22). The relevant modes divide the $\boldsymbol{k}$-space into

[26] In fact, this condition is not essential. We could as well consider more general sets $\operatorname{supp}\hat{F}^{(0)}$.

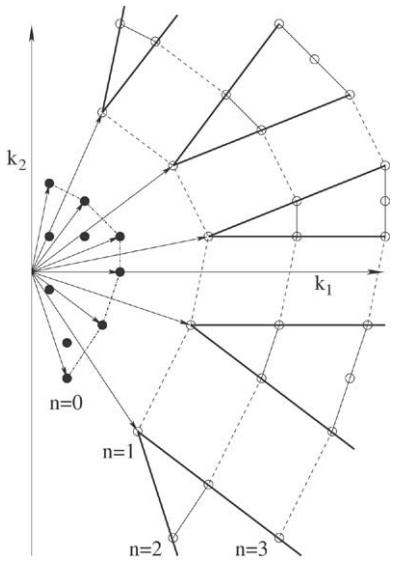

Fig. 22. Construction of relevant Fourier modes in various angular sectors. Black circles: initial modes; dash-dotted lines: boundary of the Newton polytope of the initial modes; white circles: higher-order modes associated to nth generation. Thick lines show the edges of the various angular sectors.

angular sectors, analogously to the three-mode case presented above.

Let now $\boldsymbol{k}'$ and $\boldsymbol{k}''$ be two relevant modes defining an angular sector such that $\boldsymbol{k}' \wedge \boldsymbol{k}'' > 0$. The vectors $\boldsymbol{k}'$ and $\boldsymbol{k}''$ define an angular sector in the $\boldsymbol{y}$-space such that $k_2'/k_1' \leq y_2/y_1 \leq k_2''/k_1''$. For these directions the leading-order terms in $\Psi_n(\boldsymbol{z})$ are proportional to $\mathrm{e}^{(n'\boldsymbol{k}'+n''\boldsymbol{k}'')\cdot\boldsymbol{y}}$ with $n', n'' \geq 1$ and $n' + n'' = n + 1$; the terms corresponding to other Fourier modes are subdominant. Clearly, we would have obtained the same dominant terms if we had started from just the two initial modes $\boldsymbol{k}'$ and $\boldsymbol{k}''$. We can now apply the similarity ansatz, shifting $\boldsymbol{k}' \cdot \boldsymbol{y}$ and $\boldsymbol{k}'' \cdot \boldsymbol{y}$ by $\ln t$. Let us remark that while it is possible to eliminate the time variable by a global similarity ansatz for two-mode asymptotics, it is in general impossible to do so for more than two modes.

In the exceptional cases where two or more relevant modes have the same length one must take into account the fact that the Fourier coefficient of their sum vanishes. The description of the leading-order contributions in the nth generation becomes slightly more involved than in the generic case, but the leading-order behavior in a fixed direction y_2/y_1 is still dominated by two-mode asymptotics.

Summarizing, we have shown that the study of the short-time asymptotics of Euler flows with multimode initial conditions can be reduced to the analysis of various two-mode asymptotics in angular sectors defined by a suitable set of relevant initial modes, namely those on the boundary of the Newton polytope of the initial modes.

References

[1] And it bubbles and seethes, and it hisses and roars, As when fire is with water commix'd and contending, And the spray of its wrath to the welkin up-soars, And flood upon flood hurries on, never-ending (translation by Edward, Lord Lytton).

[2] L. Euler, Principes généraux du mouvement des fluides, Histoire de l'Académie des Sciences et des Belles-Lettres de Berlin 11 (1755) 1757, 274–315.

[3] A.J. Majda, A.L. Bertozzi, Vorticity and Incompressible Flow, Cambridge University Press, Cambridge, 2000.

[4] U. Frisch, T. Matsumoto, J. Bec, Singularities of the Euler equation? Not out of the blue! J. Stat. Phys. 113 (2003) 761–781.

[5] E. Hölder, Über die unbeschränkte Fortsetzbarkeit einer stetigen ebenen Bewegung in einer unbegrenzten inkompresiblen Flüssigkeit, Math. Z. 37 (1933) 727–738.

[6] W. Wolibner, Un théorème sur l'existence du mouvement plan d'un fluide parfait, homogène, incompressible, pendant un temps infiniment long, Math. Z. 37 (1933) 698–726.

[7] C. Bardos, S. Benachour, M. Zerner, Analyticité des solutions périodiques de l'équation d'Euler en deux dimensions, C. R. Acad. Sci. Paris 282 A (1976) 995–998.

[8] S. Benachour, Analyticité des solutions de l'équation d'Euler en trois dimensions, C. R. Acad. Sci. Paris 283 A (1976) 107–110.

[9] S. Benachour, Analyticité des solutions des équations d'Euler, Arch. Ration. Mech. Anal. 71 (1976) 271–299.

[10] C. Sulem, P.L. Sulem, H. Frisch, Tracing complex singularities with spectral methods, J. Comput. Phys. 50 (1983) 138–161.

[11] U. Frisch, Turbulence, the Legacy of A.N. Kolmogorov, Cambridge University Press, Cambridge, 1995.

[12] T. Matsumoto, J. Bec, U. Frisch, The analytic structure of 2D Euler flow at short times, Fluid Dyn. Res. 36 (2005) 221–237.

[13] G.I. Taylor, A.E. Green, Mechanism of the production of small eddies from large ones, Proc. R. Soc. A 158 (1937) 499–521.

[14] M.E. Brachet, D.I. Meiron, S.A. Orszag, B.G. Nickel, R.H. Morf, U. Frisch, Small-scale structure of the Taylor–Green vortex, J. Fluid Mech. 167 (1983) 411–452.

[15] S. Kida, Three-dimensional periodic flows with high-symmetry, J. Phys. Soc. Japan 54 (1985) 2132–2136.

[16] R.B. Pelz, Y. Gulak, Evidence for a real-time singularity in hydrodynamics from time series analysis, Phys. Rev. Lett. 79 (1997) 4998–5001.

[17] C. Cichowlas, M.E. Brachet, Evolution of complex singularities in Kida–Pelz and Taylor–Green inviscid flows, Fluid Dyn. Res. 36 (2005) 239–248.

[18] S. Tanveer, C.G. Speziale, Singularities of the Euler equation and hydrodynamic stability, Phys. Fluids A 5 (1993) 1456–1465.

[19] R.E. Caflisch, Singularity formation for complex solutions of the 3D incompressible Euler equation, Physica D 67 (1993) 1–18.

[20] M.J. Shelley, A study of singularity formation in vortex sheet motion by a spectrally accurate vortex method, J. Fluid Mech. 244 (1992) 493–526.

[21] R. Krasny, A study of singularity formation in a vortex sheet by the point-vortex approximation, J. Fluid Mech. 167 (1986) 65–93.

[22] J. Weiss, M. Tabor, G. Carnevale, The Painlevé property for partial differential equations, J. Math. Phys. 24 (1983) 552–559.

[23] D.W. Moore, The spontaneous appearance of a singularity in the shape of an evolving vortex sheet, Proc. R. Soc. Lond. A 365 (1979) 105–119.

[24] G.F. Carrier, M. Krook, C.E. Pearson, Functions of a Complex Variable: Theory and Technique, McGraw-Hill, New York, 1966.

[25] A.K. Tsikh, Conditions for absolute convergence of series of Taylor coefficients of meromorphic functions of two variables, Math. USSR Sbornik 74 (1993) 336–360.

[26] A.G. Orlov, On asymptotics of Taylor coefficients of rational functions of two variables, Russian Math. (Iz. Vuz) 37 (6) (1993) 23–30 (translated from: Izv. Vuzov Mat. 37 (6) (1993) 26–33).

[27] A.G. Orlov, About asymptotics of Taylor coefficients of algebraic functions, Siberian Math. J. 35 (1994) 1125–1137 (in Russian).

[28] D.H. Bailey, A fortran-90 based multiprecision system, RNR Technical Report, RNR-94-013, 1995. See also http://crd.lbl.gov/~dhbailey/.

[29] P. Wynn, The rational approximation of functions which are formally defined by a power series expansion, Math. Comput. 14 (1960) 147–186.

[30] D. Shanks, Non-linear transformations of divergent and slowly convergent, sequences, J. Math. Phys. 34 (1955) 1–42.
[31] J. van der Hoeven, Algorithms for asymptotic interpolation, J. Symbolic Comput. (2006) (submitted for publication). Preprint 2006-12 Dep. Math. Univ. Paris-Sud. See also http://www.math.u-psud.fr/~vdhoeven/Publs/2006/interpolate.ps.gz.
[32] C.M. Bender, S.A. Orszag, Advanced Mathematical Methods for Scientists and Engineers, McGraw-Hill, 1978.
[33] P. Dienes, The Taylor Series, an Introduction to the Theory of Functions of a Complex Variable, Oxford University Press, 1931.
[34] B.V. Shabat, Introduction to Complex Analysis Part II: Functions of Several Variables, American Mathematical Society, 1992.
[35] W. Pauls, T. Matsumoto, Lagrangian singularities of steady two-dimensional flows, Geophys. Astrophys. Fluid Dyn. 99 (2005) 61–75.
[36] I. Gelfand, M. Kapranov, A. Zelevinsky, Discriminants, Resultants and Multidimensional Determinants, Birkhäuser, Boston, 1994.
[37] J. van der Hoeven, Relax, but don't be too lazy, J. Symbolic Comput. 34 (2002) 479–542.
[38] K. Itakura, A. Uno, M. Yokokawa, M. Saito, T. Ishihara, Y. Kaneda, Performance tuning of a CFD code on the Earth Simulator, NEC Res. Dev. 44 (2003) 115–120.
[39] Y. Kaneda, T. Ishihara, M. Yokokawa, K. Itakura, A. Uno, Energy dissipation rate and energy spectrum in high resolution direct numerical simulations of turbulence in a periodic box, Phys. Fluids 15 (2003) L21–L42.